MASTER THESIS

QUANTIFICATION AND PREDICTION OF HISTORY-DEPENDENT MUSCLE PROPERTIES

Nadia T.D. Sproates BSc

EXAMINATION COMMITTEE
C.P. Cop MSc
prof. dr. ir. M. Sartori
dr. E.H.F. van Asseldonk

UNIVERSITY OF TWENTE.

OCTOBER
2023

Acknowledgements

I would like to express my deepest gratitude to my daily supervisor, Pablo Cop, who made this work possible. His insightful guidance, significant support, and valuable feedback guided me through this research. Moreover, he provided a safe work environment in which he reminded me that mental well-being is also an important aspect of the process. Also, I am sincerely grateful to the other members of my graduation committee, Professor Massimo Sartori and Professor Edwin van Asseldonk, for their feedback and interest in my research.

Thanks should also go to my fellow students, and "een stelletje negen studenten" in specific, for their moral support and the card-game sessions during the breaks. I am also grateful to the other Master's and PhD students of the faculty of Neuromechanical Modelling and Engineering Lab for arranging Master meetings which provided valuable feedback. Lastly, I would like to thank my family and my boyfriend for their belief in me. Their emotional and mental support played a crucial role in the completion of this thesis.

Abstract

History-dependent muscle properties, i.e. residual force enhancement (rFE) and residual force depression (rFD), are phenomena that are dependent on the previous state of the muscle, specifically the muscle's length. rFE is characterized by an increase of steady-state force following active eccentric contraction compared to steady-state isometric force at the corresponding length, whereas rFD is characterized by a decrease in steady-state force following active concentric contraction. These history-dependent muscle properties have been extensively investigated. However, *in vivo* measurements yielded conflicting outcomes, leading to uncertainties regarding the characteristics of these muscle properties. This study aimed to quantify the influence of the operation region of the force-length relationship on rFE and rFD, as well as to quantify the influence of the muscle fiber-type composition of the muscle on rFE and rFD. Additionally, the occurrence of rFE on the tibialis anterior (TA) is attempted to be predicted with machine learning classifiers based on the acquired datasets.

Five subjects performed isometric, lengthening, and shortening contractions at 15.0-20.0 %MVC of the TA at two different ankle angles for the assessment of the influence of the operating region. The chosen ankle angles were subject-specific and ensured that the TA was operating at both the ascending limb and plateau region. For the assessment of the muscle fiber-type composition, six subjects performed isometric, lengthening, and shortening contractions of the TA, primarily composed of fiber type II, and the soleus (SOL), primarily composed of fiber type I, at 7.5-12.5 %MVC. The obtained data measured on the TA are all used as input for six different machine learning classifiers to predict the occurrence of rFE. To assess the influence of the input parameters, one parameter was excluded from the training data one by one.

No statistical differences were found regarding the influence of both the operating muscle's region and the fiber-type composition on the obtained rFE and rFD. However, on average, rFE was $3.98 \pm 1.20\%$ higher on the plateau region and $4.73 \pm 4.67\%$ higher on the TA, respectively. Additionally, more subjects were categorized as responders measuring on the plateau and on the TA. Regarding the machine learning classifiers, three classifiers, i.e. Linear Discriminant Analysis (LDA), Logistic Regression (LR), and Support Vector Machine (SVM), exhibited the highest overall performance, each achieving an f_1 score greater than 0.8. Excluding muscle activation parameters from the training data, resulted in a decrease in performance. When excluding the normalized ankle angle, only LR showed a decrease in performance. These results indicated no discernible relation between rFD and the operating muscle's region or the muscle fiber-type distribution. However, the findings suggested that rFE may be better captured when measured on the TA and on the plateau region, although further confirmation is required through future research. Understanding these history-dependent muscle properties contributes to a better overall understanding of the biomechanics of human movements and could improve biomechanical models and rehabilitation programs.

1 Introduction

1.1 Background

1.1.1 Muscle structures

Human movement is often associated with health, as it contributes to improving the physical and mental health of an individual [1]. It is advantageous for preventing diseases and also for rehabilitation. Studying the biomechanics and kinesiologic components of human movement is essential for, i.e., improving rehabilitation programs and the origin of biomechanical-related disorders. Skeletal muscles are the essential body structures responsible for generating force for maintaining posture and generating motion [2]. Due to the importance of human motion, scientists are seeking to understand the biomechanics of movements, where the first research goes way back in time. Leonardo da Vinci was the first scientist to dissect a body to study the functional anatomy of the human body [3]. However, it was the research of Luigi Galvani (1737-1798) that was essential for the origin of muscle contraction and neurosciences [4]. In his research, he found that the legs of a frog twitch due to electrical stimulation.

After years of studying the underlying mechanisms of human movements, knowledge is gained on the anatomical and biomechanical structures of muscles. Muscle tissue is organized in a hierarchical structure [5]. The muscle itself contains multiple fascicles, which are bundles containing muscle fibers. A single muscle fiber contains, in turn, multiple myofibrils, which are accountable for the contractile motion of a muscle. A sarcomere is a specific region of the myofibril and is the smallest contractile unit of a muscle fiber. A well-accepted theory for skeletal muscle fiber contraction is the sliding filament model of a sarcomere and the cross-bridge theory [6]. This model consists of a thick and thin filament called myosin and actin, respectively. A myosin filament contains heads that can form connections with actin. These connections are called cross-bridges, and the formation of this phenomenon results in contractile motion. During contraction, the filaments slide past each other, resulting in shortening of the entire sarcomere. Each sarcomere also contains an elastic filament called titin. It maintains the organizational structure of myosin and actin and provides passive force production when the sarcomere is excessively stretched [7].
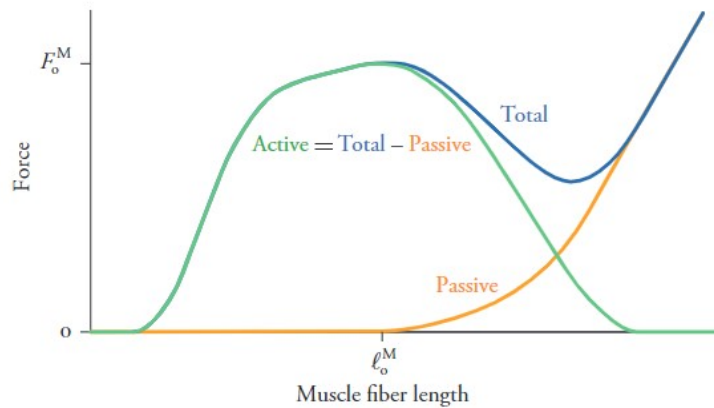

Figure 1: The force-length relationship can be determined by dividing the curve into active force generation, due to cross-bridge formations, and passive force generation, due to the engagement of titin [8].

The ability of a sarcomere to generate force is, among other things, dependent on its length. The length of the sarcomere affects the overlap of the myosin and actin, which, in turn, influences the number of cross-bridges that can be formed. The tension or generated force of the sarcomere increases with the number of cross-bridges. The force-length relationship (Figure 1) [8] describes the active force generation in relation to the sarcomere length in activated muscles. This curve has three distinct regions: the ascending limb, plateau, and descending limb region. The ascending limb region describes an increase in force with increasing sarcomere length. Initially, actin and myosin are more overlapped, leading to fewer attachment sides for cross-bridge formations. The increase in force with increasing sarcomere length is the result of an increase in cross-bridge formation as the sarcomere is less overlapped. The plateau region represents the optimal region, where the produced force is at its maximum and does not change with the number of cross-bridges as all attachment sides are available. In the descending limb region, the force decreases with increasing sarcomere length, as fewer cross-bridges can be formed. Actin and myosin are not fully overlapped, resulting in fewer attachment sides. In this region, passive forces are generated by the engagement of titin when the sarcomere is stretched.

Important to note is that not all muscle fibers have the same contraction speed and force generation. In the human body, in general, three types of muscle fibers can be distinguished: type I (slow-twitch), type IIA (fast-twitch type A), and type IIX muscle fibers (fast-twitch type X) [9]. While the type I muscle fiber is more fatigue-resistant, both type II muscle fibers are capable of contracting more quickly than type I muscle fibers. Type I fibers are recruited for endurance exercises when oxygen is available for energy production. Type II fibers, both type IIA and type IIX, are recruited for more force-demanding activities in the absence of an adequate amount of oxygen. Type IIA fibers are often recruited for higher-intensity endurance activities, while type IIX are recruited for explosive events. However, it appears that type IIX muscle fibers are not easily activated. With this in mind, the subdivision of type II is not considered in this thesis. Within the different muscle fibers, the properties of titin differ from one another. Previous research has found that the stiffness of titin is higher for type II muscle fibers [10], which, in turn, influences the passive force generation. Even though the sliding filaments model and cross-bridge theory are often used to explain the properties of skeletal muscles, the origin of some specific muscle properties remains unknown. [11].

1.1.2 History-dependent muscle properties

Not all muscle properties are accounted for in the currently accepted muscle models. Among those are history-dependent muscle properties [12, 13]. History-dependent properties in muscles include residual force enhancement (rFE) and residual force depression (rFD) (Figure 2).

Both phenomena are dependent on the previous state of the muscle, specifically its length. rFE is characterized by an increase of steady-state force following active eccentric contraction compared to steady-state isometric force at the corresponding length [14]. This enhancement is believed to be produced by titin, which exhibits spring-like properties. During the lengthening of the sarcomere, titin is stretched and consequently increases the passive force generation. During active lengthening of the muscle, calcium is used for triggering muscle force production. It is assumed that titin is also calcium-dependent resulting in interactions with other proteins. Presumably, calcium results in titin binding to actin at specific binding sites. Consequently, the stiffness of titin increases after the binding to actin [15, 16]. This increase in stiffness and the passive forces generated by titin is thought to be contributing to rFE [17].

On the other hand, rFD is observed as a decrease of steady-state force following active concentric contraction [18]. Similar to rFE, titin is associated with rFD as well. It is hypothesized that titin directly blocks the formation of new cross bridges during active muscle shortening. The inhibition of cross-bridge formation is likely to be the primary mechanism contributing to rFD [18]. However, despite extensive research, the exact physiological origin of both rFE and rFD remains unknown.
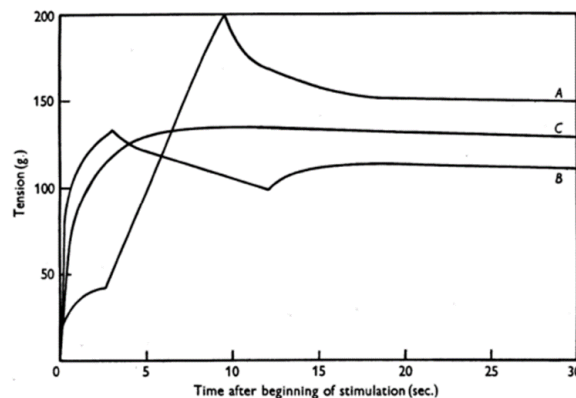

Figure 2: Schematic representation of rFE and rFD. Line A shows an increase in steady-state isometric force following active lengthening of the muscle (rFE) compared to a purely isometric contraction, which is represented by line C. Line B shows a decrease in steady-state isometric force following active shortening of the muscle (rFD) compared to a purely isometric contraction [19].

1.1.3 Machine learning

The occurrence of rFE has been extensively investigated in both *in vitro* and *in vivo* experiments. as will be discussed in Section 1.2.1. Especially *in vivo*, the results of the experiments are not consistent, and not all subjects exhibit rFE [20, 21]. Consequently, it is challenging to predict the occurrence of rFE, especially *in vivo*. Being able to predict rFE provides more insight into the nature of rFE, the related parameters, and the reasoning why some subjects do not exhibit rFE while other subjects do. As the *in vivo* properties are not yet fully understood, measurement data can be used to predict the occurrence of rFE. Machine learning is a promising technique for predicting the occurrence and determining the influencing parameters of history-dependent muscle properties.

Machine learning is a data-driven technique often used to make predictions or classifications. This technique enables systems to learn and to improve based on measurement data [22]. The general idea of machine learning is that specific learning algorithms are able to build models given input data, i.e. training data, which is validated against test data. These models then return predictions of new data. Especially with the increasing complexity of datasets, i.e. an increasing amount of data and an increasing amount of predicting variables, the demand for machine learning models increases [23]. While there are multiple different algorithms that can be applied, there is not one common algorithm that fits all data. The decision of what kind of algorithm to use depends on the dataset itself and the type of prediction that is required [24]. In this thesis, six machine learning algorithms were investigated. The algorithms are attempted to be explained by means of an example. Imagine a classification problem where a pill needs to be classified being either red or blue based on its weight.

Gaussian Naive Bayes
Naive Bayes is an algorithm that uses Bayesian probability to calculate the likelihood of a certain event to happen [25]. This classifier is popular among the anti-spam filters for e-mails [26]. The data is assigned to a certain class, which is the group the input data belongs to. For the given example, the class is either red or blue. The algorithm is based on the following formula [24]:

$$P(c|x) = \frac{P(x|c) \cdot P(c)}{P(x)}, \tag{1}$$

with $P(c|x)$ the posterior probability, $P(x|c)$ the likelihood of the weight of the pill given its color, $P(c)$ the probability of the class, i.e. the pill being either red or blue based on the training data, and $P(x)$ the probability of the prior predictors. The posterior probability is the eventual outcome that will be used for the classification. First, the probability of the class is the initial guess of the classification, e.g., the color of the pill being either red or blue. This initial guess is often the probability calculated based on the training data. Then, this initial guess is multiplied by the likelihood of the color of the pill being red or blue given a certain weight. This gives two posterior probabilities. The input data is classified as the same class of the posterior probability with the highest value, e.g. if the probability of the color being red is higher than the probability of being blue, the pill is classified as the color red.

Gaussian Naive Bayes assumes a Gaussian distribution of the dataset and is often used for handling continuous data. Moreover, it is assumed that each input parameter is independent of the others. Important to note is that the performance of the classifier is correlated with this data distribution. The model conducts better predictions on a normally distributed dataset [27].

Linear- and Quadratic Discriminant Analysis
Linear Discriminant Analysis (LDA) and Quadratic Discriminant Analysis (QDA) are two classification methods based on statistical and probabilistic learning [28]. These algorithms can be derived for binary and multivariate classification problems. The formula on which both LDA and QDA are based is the probability density function for multivariate normal distribution [29]:

$$f(x|\mu, \Sigma) = \frac{1}{\sqrt{(2\pi)^p |\Sigma|}} \exp\left(-\frac{(x-\mu)^T \Sigma^{-1} (x-\mu)}{2}\right), \tag{2}$$

where $x = (x_1, x_2, ..., x_p)$ is the independent variable, $\mu = (\mu_1, \mu_2, ..., \mu_p)$ is the mean of the independent variable, and Σ is the covariance matrix.

LDA assumes for binary classifications, i.e. classifying the dataset into two groups, that both covariance matrices are equal. Given this property and after simplification of Equation 2, the linear discriminant function of binary classification can be obtained [29]:

$$\delta(x) = 2\left(\Sigma^{-1}(\mu_2 - \mu_1)\right)^T x + \left((\mu_2 - \mu_1)^T \Sigma^{-1}(\mu_2 - \mu_1)\right) + 2\ln\left(\frac{\pi_2}{\pi_1}\right). \tag{3}$$

The classes are determined by the value of $\delta(x)$. $\delta(x)$ can either be positive or negative each resulting in a different class, e.g. if $\delta(x)$ is positive the pill is classified as red, and if $\delta(x)$ is negative the classification is the pill being blue.

QDA assumes unequal covariance matrices for a binary classification, which results in the following formula [29]:

$$\delta(x) = x^T \left(\Sigma_1 - \Sigma_2\right)^{-1} x + x \left(\Sigma_2^{-1}\mu_2 - \Sigma_1^{-1}\mu_1\right)^T x + \left(\mu_1^t\Sigma_1^{-1}\mu_1 - \mu_2^t\Sigma_2^{-1}\mu_2\right) + \ln\left(\frac{|\Sigma_1|}{|\Sigma_2|}\right) + 2\ln\left(\frac{\pi_2}{\pi_1}\right). \quad (4)$$

Assumptions for the use of these two classifiers are that the dataset should follow the multivariate normal distribution, and multi-collinearity, i.e. correlation between the variables, should be excluded [30].

Logistic Regression
Logistic Regression (LR) is often used to calculate the likelihood of something happening based on given input data. This method uses a regression equation to fit the data by means of logarithmic terms in order to avoid the assumption of linearity [31]. The formula that will be modeled is given with the following [32]:

$$\log\left(\frac{\pi}{1-\pi}\right) = \beta_0 + \beta_1 x_1 + \beta_2 x_2 + ... + \beta_m x_m, \quad (5)$$

where π represents the probability, β the regression coefficients, and x the input variables. The goal is to fit the curve accurately to minimize the negative log-likelihood, meaning that the likelihood will be maximized [33]. The curve obtained with LR has an S-shape between zero and one which represents the probability of an event happening. On default, the boundary of the two groups, e.g. having a pill with the color red or blue, is set on a probability of 0.5. If the value is smaller than 0.5, the pill is blue based on the input parameters. This technique is also applicable when more than one predictor is available.

Support Vector Machine
Support Vector Machine (SVM) (Fig. 3) is a commonly used machine learning algorithm in computer science and engineering communities [34]. SVM is used for classification while mapping the training data. Imagine the blue cluster of data points, is the data representing the weight of the blue pills, and the red cluster represents the weight of the red pills. When using this technique the margins between the two classes, i.e. the blue and the red pills, are determined by support vectors, which are data points on the edge of the clusters. With a maximized margin between the two data clusters, the optimal hyperplane can be determined. This optimal hyperplane is the boundary between the data clusters and has an equal distance between the support vectors of both clusters [24]. Considering Figure 3, the pill is classified as red as the weight is mapped to the right of the optimal hyperplane. In general, SVM algorithms solve linear problems. In case the analyzed data is non-linear, kernel functions can be used to transform the data such that linear classifiers can be applied [35].
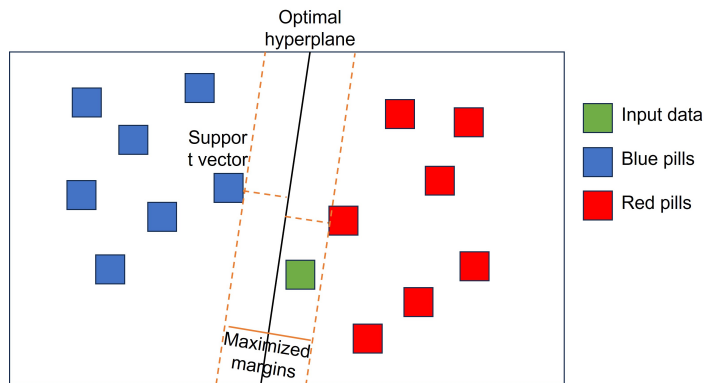

Figure 3: Schematic overview of the functionality of the machine learning algorithm of SVM. The optimal hyperplane is the plane that has the maximum margin with respect to the support vectors.

K-Nearest Neighbor
K-Nearest Neighbor (KNN) is also an algorithm often used for classification purposes [24, 36]. The classifier uses the training data for comparison with the unclassified input. This means the training data will be mapped based on the weight of the pills. Each training data point is assigned to a classification, i.e. the pill being red or blue. The input is classified to the value with the training data that shows the most resemblance [36]. The measure that is used, is called the distance function which is most commonly the Euclidean Distance [36, 37]:

$$d_{Euclidean}(x, y) = \sqrt{\sum_i (x_i - y_i)^2}. \tag{6}$$

After the determination of the distances between the input data and the training data, the input is assigned to the class of the nearest neighbors of the training data. In other words, the pill is classified as red if a training data point with the most similar weight belongs to the class of red pills. The number of neighbors that are considered is determined by the k-factor. If k is larger than 1, the majority class of the neighbors is assigned to the input [38]. Considering Figure 4, the pill is classified as blue as the majority of the nearest neighbors belong to the blue class when k is 3.
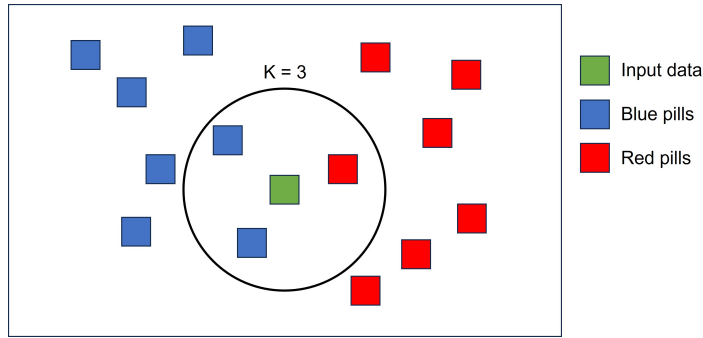

Figure 4: Schematic overview of the functionality of the machine learning algorithm KNN.

1.2 State of the art

1.2.1 Properties of rFE and rFD

Many experiments have been conducted both *in vitro* and *in situ* to establish the properties of rFE and rFD. Important outcomes from previous *in vitro* experiments regarding rFE show that this phenomenon is dependent on the stretch amplitude and is velocity-independent [11]. Moreover, rFE occurs over the entire force-length relationship [11]. Presumably, rFD is dependent on the produced force and stretch amplitude, but also velocity-independent [39].

Currently, research is underway to investigate the effects of rFE and rFD *in vivo* [11, 18]. It is likely that these phenomena occur during daily movements in humans. The *in vivo* measurements are often performed with joint torque and angle as proxies of muscle force and length, respectively. However, other factors, such as the involvement of other muscles and tendons, might also influence the measured joint torque and angle. Therefore, the functionality of the phenomena in the human body is not fully understood yet, while experiments on single muscles and single sarcomeres yield consistent and clear results [11, 18].

Additionally, while measuring for rFE *in vivo*, responders and non-responders are observed [40]. On average, 25 % of the participants do not exhibit rFE involving voluntary contractions. However, non-responders are not observed *in situ* and *in vitro*, nor when muscles are electrically stimulated [40, 41]. Moreover, Paternoster *et al.* (2021) [41] questioned the existence of true non-responders, as inconsistency is found within individuals. This inconsistency might be due to other confounding factors, like varying sensor placement or voluntary contraction. It remains unclear why some participants do not show rFE. Recent articles regarding rFD did not find non-responders or find a small number of non-responders in their study [42–44].

Some of the findings from *in vivo* measurements indicate that the magnitude of rFE is likely to depend on the region of the force-length relationship the muscles are operating on. Evidence suggests that the magnitude of rFE is decreased in the ascending limb region, while an increase in rFE can be found in the descending limb region [42]. This observation is likely due to the engagement of titin at longer muscle lengths. This research is, however, limited by the decision to measure two different ankle angles for each subject, not taking into account that the force-length relationship is subject-specific. This can result in subjects operating in a different region than assumed. Regarding rFD, current articles do not mention a similar relation between the operating region and rFD [18], suggesting that this relation is unlikely to influence the magnitude of rFD. Another notable outcome is that the activation level does not influence the magnitude of rFE or rFD [45].

Additionally, Ramsay *et al.* (2010) [46] examined the contribution of non-contractile proteins, e.g. titin, which is responsible for the passive force generation. Within this research, two rat muscles with different fiber-type compositions were compared, one with relatively more type I fibers and the other with more type II fibers. They found a significant increase in rFE for the muscle with relatively more type II fibers, most likely due to the higher proportion of the passive tension that is generated. On the contrary, Fukutani and Herzog (2020 and 2022) [47, 48] also compared two different muscles with distinct fiber-type distributions, specifically the rabbit's psoas (type II), and the soleus (type I), but no significant difference was found. Pinnell *et al.* (2019) [40] investigated rFE on single human muscle fibers, obtained from the vastus lateralis. However, no difference in the magnitude of rFE was found between the type I and type II muscle fibers. Therefore, it remains inconclusive whether muscle fiber types indeed influence the magnitude of rFE.

The influence of different fiber-type compositions on rFD was also examined by Joumaa *et al.* (2015) [49]. The rabbit soleus and psoas were assessed. The outcome of this research showed a greater rFD for type II muscle fibers than type I fibers when measuring at the same absolute speed, i.e. fiber lengths per second. Pinnell *et al.* (2019) [40] also measured the occurrence of rFD on single human muscle fibers. This research found no significant difference between the two fiber types. The conflicting results indicate that the relationship between the muscle fiber-type and the occurrence of rFD is uncertain.

1.2.2 Predicting models

As said, rFE and rFD have been widely studied *in vitro* and *in situ*. Experimental studies have been executed to gain more insights into the underlying mechanisms of rFE and rFD and the properties of these two phenomena [11]. Most hypotheses are based on the sliding filament and the cross-bridge theory. However, no current model is able to fully explain the origin and mechanisms responsible for the occurrence of rFE and rFD [50].
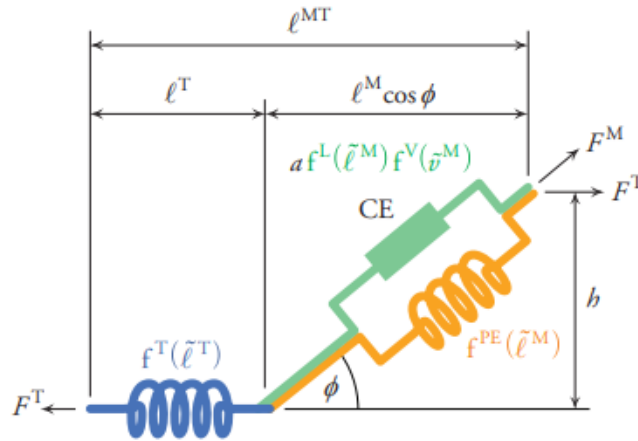

Figure 5: Schematic overview of the classic Hill-type muscle model. The force generated by the muscle is described by the active contractile element (CE) and a passive elastic element (PEE/f^{PE}) at a pennation angle of ϕ. The tendon force is described as the tendon passive element (TEE/f^T) [8].

Musculoskeletal simulations are often based on the Hill-type muscle model [51]. This phenomenological model describes the dynamics of a muscle-tendon unit. This model consists of three components, specifically an active contractile element (CE), a passive elastic element (PEE), and a tendon elastic element (TEE), which describes the generated muscle force (Figure 5) [8]. The CE is the component that describes the active force generation, specifically the force-length and the force-velocity relationship. The CE operates in parallel with the PEE, which describes the passive force generation of the elastic elements within the sarcomere, i.e. titin. The TEE component operates in series with CE and PEE and describes the passive force generation of the tendon itself [52]. The traditional Hill-type model is purely based on a single state of the muscle, specifically at the instantaneous muscle length, and neglects some muscle features, like size-dependency, activation-dependency, and history-dependency [53]. Some articles tried to improve the Hill-type muscle model by adding history-dependent features [52–54]. McGowan *et al.* (2013) [54] included both a rFE and a rFD component to the Hill-type muscle model, where rFE is mainly determined by the change in muscle length, and rFD is a function of the net work [52]. Ross *et al.* (2018) [55] also implemented a history-dependent muscle property within the Hill-type muscle model. The history-dependent component is implemented in parallel to the CE and the PEE and describes both rFE and rFD. In the case of active lengthening of the muscle,

the rFE is calculated based on the active stretch. The formula goes as follows:

$$F_{FE} = F_0 \left[\frac{l_m - l_e}{l_e} \right] \hat{E} \left(\frac{l_e}{l_0} \right), \tag{7}$$

where F_0 represents the maximum isometric force, $\hat{E}$ the normalized elastic modulus dependent on the initial muscle length, l_e, and the muscle length after active stretch, l_m. In the case of active shortening, the rFD is calculated based on the net work of the muscle across various scales of muscles, calculated with the following formula:

$$F_{FD} = -F_0 \hat{C}_{FD} \hat{W}_c, \tag{8}$$

where $\hat{C}_{FD}$ represents the non-dimensional force depression coefficient, and $\hat{W}_c$ the non-dimensional work. The relationships described in the phenomenological models are mainly based on *in situ* and *in vitro* measurements, whereas the used parameters, i.e. the muscle length and the mechanical work, are challenging to capture *in vivo*.

Some articles describe the development or application of mathematical muscle models accounting for rFE [50, 56–58]. These models describe the mechanical behavior of skeletal muscles for predicting whether rFE occurs. Campbell *et al.* (2011) [50] used a half-sarcomere model that showed rFE. This model confirmed some established properties, like the independence of stretch velocity and dependence on stretch amplitude. Another predicting model is of Heidlauf *et al.* (2016) [57], which is a mechanical model that also considers rFE in static situations based on the mechanical behavior of titin. The titin model is proposed by Rode *et al.* (2009) [56], where a sticky-spring mechanism is integrated into the Hill-type muscle model. This model is useful for simulating both rFE and rFD. Schappacher-Tilp *et al.* (2015) [58] proposed a mathematical model of a three-filament sarcomere model which shows both rFE and rFD to some extent.

These models, however, are specifically used for obtaining insights into mainly rFE on the sarcomere level and the underlying mechanisms. These models are based on *in vitro* and *in situ* measurements with the established properties of rFE and rFD, but also with input measures, like the muscle length and the number of myosin heads. Seemingly, no mathematical models are proposed for explaining the phenomena *in vivo*. Also, no articles are found regarding the history-dependent muscle properties in combination with machine learning techniques.

Machine learning algorithms, however, have been applied to disease predictions and other biological processes [59]. Several datasets were evaluated by means of machine learning models to either predict the occurrence of certain diseases or to classify patients. This technique has been applied to many different medical conditions, i.e. asthma [60], breast cancer [61], cerebral infarction [62], diabetes [63], and Parkingson's disease [64]. The machine learning models assessed in the review of Uddin *et al.* (2019) [59] often showed high performance in terms of classifying diseases. In the research of Pascual-Valdunciel *et al.* (2022) [65], machine learning algorithms were utilized for tremor detection based on electromyography (EMG) and kinematic data, whereas the assessed algorithms all showed high overall performance. These researches showed the feasibility of applying machine learning algorithms for predicting and classifying biological processes in humans and also the classification based on EMG- and kinematic data. This indicates the potential for machine learning algorithms to classify and predict history-dependent muscle properties.

1.3 Research objective

Measuring rFE and rFD *in vitro* or *in situ*, the properties of these two phenomena are well-established and consistent. However, for *in vivo* measurements, the results are rather conflicting and therefore it is unclear which factors influence the magnitude and occurrence of these history-dependent properties *in vivo*. The goal of this research is to quantify whether the influence of the operating regions of the force-length relationship and the fiber-type distribution within the muscle affect rFE and rFD. Another research objective is to obtain a predicting classifier capable of predicting the occurrence of rFE based on given input parameters.

During this research, measurements were conducted for measuring rFE and rFD in relation to the operating region and the muscle fiber-type distribution. Regarding the influence of the operating region on the force-length relationship, two ankle angles are chosen per subject, one representing the ascending limb region and the other representing the plateau region. It is hypothesized that titin is more engaged at longer muscle lengths [8, 17], resulting in a higher passive force generation. Therefore, it is assumed that rFE is better captured at the plateau region.

Contrarily, it is hypothesized that the occurrence and the magnitude of rFD are independent of the operating region of the muscle. Unlike the hypothesis for rFE, the occurrence or magnitude seems independent of passive force generation, i.e. the engagement of titin. As mentioned, cross-bridge inhibition is likely to be the main mechanism

responsible for the occurrence of rFD [18]. Therefore, it is assumed that no difference in magnitude between the two ankle angles is found.

Regarding the influence of the muscle fiber-type distribution of the different muscles, measurements are performed on two different muscles with different compositions of fiber types. It is hypothesized that a muscle with relatively more type II fibers exhibits more rFE. Due to the fast contraction of these type II fibers, titin is stiffer for maintaining the structure of the sarcomere. Consequently, more passive force is generated when titin is engaged in these fibers. Therefore, it is likely that type II muscle fibers exhibit more rFE than type I muscle fibers [10, 46].

Similar to the hypothesis regarding the operating region and rFD, it is assumed that the fiber-type composition does not influence the magnitude or occurrence of rFD. Presumably, the stiffness of titin, and consequently the passive force generation, is different for the different muscle fibers. As it is unlikely that the passive forces are influencing the occurrence or the magnitude of rFD. Therefore, it is hypothesized that the rFD is similar for both conditions.

Understanding these history-dependent muscle properties contributes to a better understanding of the biomechanics of human movement. Currently, the functionality and relevance of rFE and rFD have not been verified yet. Research suggests that the occurrence of rFE is beneficial for human movements that require high forces, like fall prevention [11]. Moreover, rFE contributes to optimizing the neuromuscular economy by reducing activation [66, 67]. Regarding rFD, some articles propose that rFD could potentially decrease the work needed for active lengthening. This, in turn, might enhance the overall work performed by a muscle during a complete cyclic shortening/lengthening movement [46, 68]. Raiteri *et al.* (2023) [69], however, found in their research that rFD and positive muscle work were only linearly related to each other in the case when the muscle was preloaded. This indicates that rFD is not always related to muscle work. Obtaining a better understanding of rFE and rFD could improve biomechanical models for rehabilitation programs and controllers for orthoses and prostheses. Specifically, EMG-based musculoskeletal models could be improved by better understanding which *in vivo* parameters contribute to the occurrence of these history-dependent muscle properties. Incorporating these muscle properties into EMG-musculoskeletal models can enhance both the accuracy of the model's predictions and its ability to replicate real-world daily movements, improving its resemblance to the desired controller behavior.

2 Materials and methods

This research project can be divided into two parts: quantification of rFE and rFD and predicting the occurrence of rFE. For both parts, the data needed to be pre-processed followed by the evaluation of the data, i.e. calculations and statistical tests. Finally, the processed data was used as input data for predicting models (Figure 6).
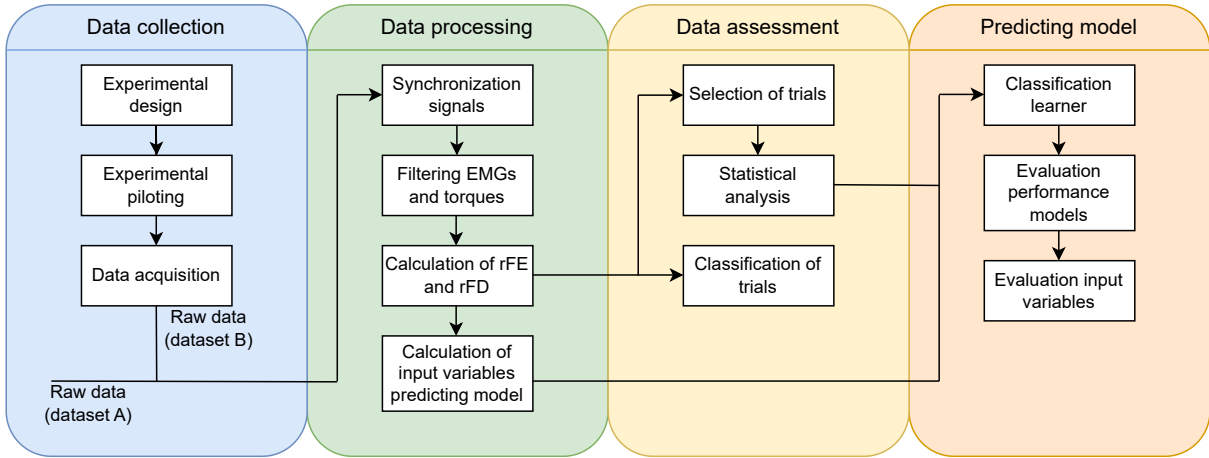

Figure 6: Schematic overview of the workflow of this research. In the first step after the acquisition of the data, the data was processed such that it was appropriate to use for the quantification and prediction of the history-dependent properties. Afterward, the data was evaluated followed by the application of a predicting model.

2.1 Participants and data acquisition

2.2 Participants

In total, eleven healthy participants were included in the experiments, who were divided into two different datasets. The first dataset (dataset A) quantifies the relation between the operating region of the force-length relationship and the occurrence and magnitude of rFE and rFD. The data acquisition was executed beforehand of this research. Five subjects with a height of 170.4 ± 8.8 cm and a weight of 68.6 ± 11.0 kg were included in the experiments. The second dataset (dataset B) was for evaluating the relation between the muscle fiber types, and the occurrence and magnitude of rFE and rFD. The data acquisition was executed during this research. Six subjects were included in dataset B, with a height of 176.7 ± 8.2 cm and weight of 74.7 ± 16.2 kg. The measurements of subject 01 of dataset B were excluded from the data analysis due to irregularities during the measurements.

2.3 Equipment

The experimental setup was similar for both datasets, where both EMG and kinetic data were obtained. The EMG activity of four lower leg muscles of the right leg was measured, which were the Tibialis Anterior (TA), the soleus (SOL), the Gastrocnemius Medialis (GM), and the Gastrocnemius Lateralis (GL). The TA and SOL were both measured with 64-channel High-Density surface EMGs (HD-EMG) electrodes (Figure 10), while the GM and GL were measured with bipolar sensors, using a TMSi Refa amplifier (TMSi, Oldenzaal, The Netherlands) with a sampling frequency of 2048 Hz. The ground electrode was placed on the Lateral Malleolus. The kinetic data for this research that was measured was ankle torque. The torque and ankle angle was measured at 2048 Hz with the Achilles Rehabilitation Device (MOOG, Nieuw-Vennep, the Netherlands). The Achilles was used to impose a change in angle to the right ankle. The ankle joint was aligned with the motor of the Achilles, while the foot was secured with straps to the footplate. The ankle angle of the Achilles was also recorded with a channel of the Refa amplifier.
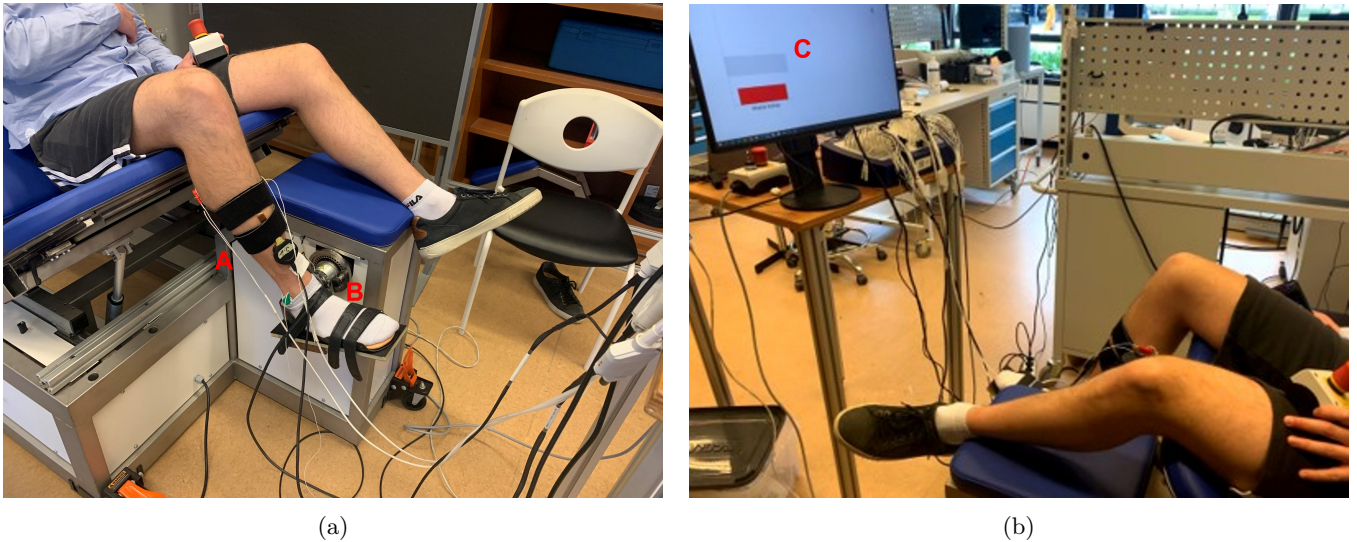
(a)

(b)

Figure 7: The experimental set-up of the history-dependent measurements. (a) depicts the experimental setup. The HD-EMG sensors (A) were placed on the TA and the SOL, while the GM and GL were measured with bipolar EMG sensors. The right foot of the subject was positioned at the footplate of the Achilles (B) for measuring torques. (b) shows the live activation target (C) of the subject during the trials. In this case, the height of the red bar represented the magnitude of the activation level of the muscle of interest. Once the red bar reached the grey target, the bar turned green. This indicated that the activation level was at the required magnitude.

2.4   Experimental protocol

The data acquisition was executed similarly for both datasets (Figure 8). In both cases, the experiment started by measuring the maximal voluntary contraction (MVC) of interest. The test subject was instructed to sit on the chair with a knee angle of ~90° and either dorsiflex or plantar flex the ankle, while the instructor provided a counterweight. The subject was then seated on the chair of the Achilles with the right foot positioned on the footplate. The range of motion (ROM) was determined for the subject by manually determining the maximal and minimal ankle angle followed by the placement of hard stops.

Afterwards, the torque-angle relationship was determined. As the torque-angle relationship (as a substitution for the force-length relationship) is subject-specific, one trial was dedicated to the determination of this relationship (Appendix A). The subject was instructed to sub-maximally contract the muscle of interest, which was either the TA or the SOL, for a duration of 5 s. The sub-maximal contraction was either 15.0-20.0 %MVC for dataset A and 7.5-12.5 %MVC for dataset B. Then a transition of 5° of the ankle angle was made, after which the subject was instructed to sub-maximally contract the muscle again. This trial ensured that ten ankle angles were measured throughout the ROM of the ankle. The sub-maximally contraction needed to be consistent throughout the entire measurement. Therefore, the subject was provided with live visual feedback on the activation level during the trial. The activation level was determined by the selection of two 2×2-grids of the HD-EMG sensor (Figure 10). By averaging each 2×2-grid and subtracting both means from each other, one EMG signal was obtained. The signal was filtered and normalized with the MVC to provide live feedback.
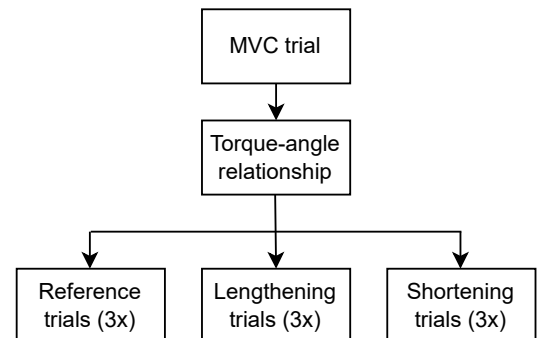

Figure 8: A schematic overview of the trials that were executed. First, the trial started with an MVC trial followed by the trial to determine the torque-angle relationship. After the execution of these trials, the history-dependent muscle property trials were performed threefold: reference, lengthening, and shortening trials. The reference trial was a purely isometric contraction. The lengthening trial initiated active lengthening of the muscle and the shortening trial initiated active shortening for measuring rFE and rFD, respectively.
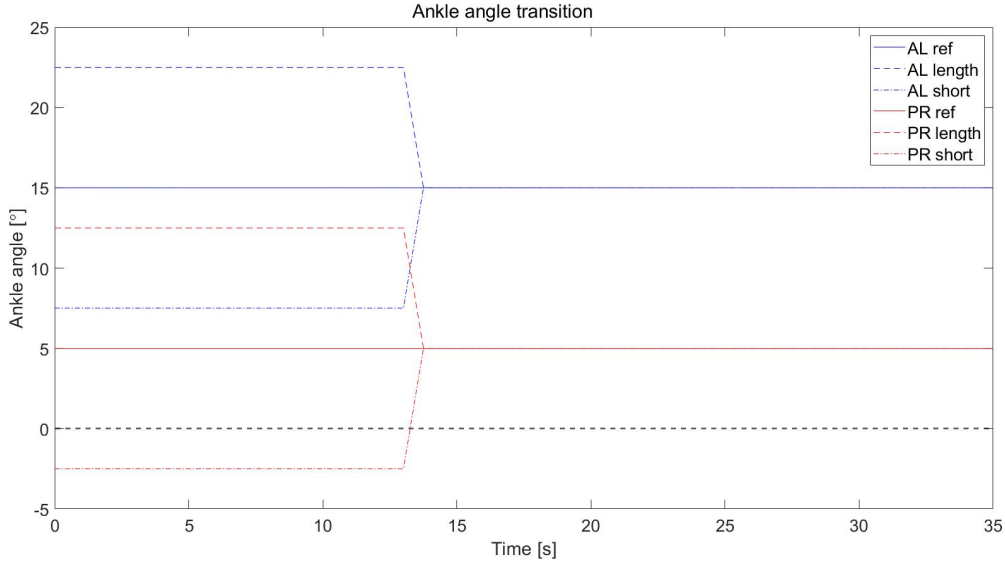
Figure 9: Ankle angle transition for the different operating muscle lengths. The positive ankle angles were in the dorsiflexed ankle position, the negative angles were in the plantar flexed angle position. The ankle angles were obtained from the experiments of subject 4 of dataset A.

The determination of the torque-angle relationship substantiated the decision on what ankle angle the trials for the history-dependent muscle properties were executed. The trials for the history-dependent muscle properties consisted of three conditions, specifically a reference, lengthening, and shortening trial. Each of these conditions was measured threefold. The first condition was the reference trial, which was an isometric contraction measured at the chosen ankle angle. The second condition was the lengthening trial. The trial started at a shorter muscle length followed by active lengthening of the muscle of interest ending at the chosen ankle angle for measuring rFE. The final condition was the shortening trial, which initiated the active shortening of the muscle of interest, i.e. for measuring rFD. In this case, the trial started with a longer muscle length followed by the shortening of the muscle ending at the chosen ankle angle (Figure 9).

Table 1: Overview of the measurement parameters regarding both dataset A and B, where dataset A assessed the influence of the muscle's operating region and dataset B assessed the influence of the muscle fiber-type distribution.

	Knee ankle (°)	Stretch amplitude (°)	Stretch velocity (° s^{-1})	Activation level (%MVC)	Duration (s)
Dataset A	150	7.5 and 15.0	10.0	15.0-20.0	38
Dataset B	110	7.5	10.0	7.5-12.5	38

2.4.1 Dataset A - Operating region

While the experimental protocol was almost identical for the operating region- and the fiber-type experiments, some experimental parameters were different (Table 1). Regarding dataset A, the subject's knee angle was approximately 150° with 180° being the fully extended knee position. The knee angle was measured manually by means of a goniometer. The primary muscle of interest was the TA, as it is the main muscle responsible for dorsiflexing the foot [5]. The measurements of the phenomena of rFE and rFD were executed at two different muscle lengths, each representing a distinct operating region of the force-length relationship. By means of the torque-angle relationship, one angle was selected from the ascending limb and the other from the plateau region. Afterward, the trials, consisting of three conditions, for measuring the history-dependent muscle properties were executed.

The subjects were instructed to maintain a constant activation level of the TA between 15.0-20.0 %MVC throughout the entire measurement of approximately 38 s by dorsiflexing the ankle. This activation level was determined by means of trial and error such that fatigue was avoided during measuring. Also, another research has been executed on 30 %MVC while measuring for 30 s and no fatigue has been observed [66]. The stretch velocity was kept consistent for all trials at 10 ° s^{-1}. The stretch amplitude was predominantly kept at 7.5°, except for the ascending limb trials of subject 2 and 3, where the stretch amplitude was 15°.

2.4.2 Dataset B - Fiber types

Regarding dataset B, the history-dependent properties were measured on two muscles, specifically the TA and the SOL. In this case, the knee angle was approximately 100°. This was to minimize the contribution of the GM and GL during plantarflexion, such that the SOL was the primary muscle producing torque at the ankle [70]. By means of the torque-angle relationship, an ankle angle for both the TA and the SOL was chosen that operates at the plateau region of the corresponding muscle. The same trials were executed threefold for both the TA and the SOL, specifically the reference, lengthening, and shortening trials. For the TA, the subjects were instructed to perform dorsiflexion, and for the SOL trials plantarflexion needed to be executed. This time, a constant activation level between 7.5-12.5 %MVC during the measurement of approximately 38 s was required, such that the torque will not exceed the maximum torque that can be applied on the Achilles during the SOL trials. The stretch amplitude and the stretch velocity were kept constant at 7.5° and $10°\,\mathrm{s}^{-1}$, respectively.

2.5 Data processing

The pre-processing of the recorded data, i.e. EMG data and data recorded with the Achilles, was performed in MATLAB (MathWorks Inc. Natick, Massachusetts, United States, version R2021b). Before the end of the measurement, the Achilles perturbs the ankle with a sinusoidal movement. This motion functions as a recognition point for synchronizing the torque and EMG data.

2.5.1 EMG data

For analyzing the EMG data, the EMGs were pre-processed by means of filtering and normalizing the signals for the four measured muscles, i.e. TA, SOL, GM, and GL (Figure 11). For the pre-processing and analyzing of the signals of the HD-EMGs, the same channels of the grid were chosen as the live visual feedback during the measurements for consistency (Figure 10).

The following steps were similar for both the HD-EMGs and the bipolar EMGs. After the synchronization and pre-processing of the HD-EMGs, the EMGs were processed by applying a second-order Butterworth high-pass filter with a cut-off frequency of 10 Hz, for the removal of low-frequency contaminants, like movement artifacts [71]. Due to the presence of powerline interference, the signal was also filtered by means of a harmonic notch filter of the fourth-order at multiplications of 50 Hz. Following was creating the EMG linear envelope by first rectifying the signal and then low-pass filtering. The low-pass filter was a second-order Butterworth filter with a cut-off frequency of 2 Hz. Finally, the baseline that was measured without any muscle activity was removed from the signals and the EMGs were normalized with the MVC of the corresponding muscle.

Figure 10: HD-EMG grid channels, seen from above when attached to the skin. The colored channels were the channels chosen for providing live feedback on the activation level of the muscle of interest.

2.5.2 Torque data

The torque data was eventually the data that will be used for the calculation of rFE and rFD. However, the raw torque data was challenging to analyze due to the presence of noise. To be able to analyze the data sufficiently, the torque data was smoothed by means of a second-order Butterworth low-pass filter with a cut-off frequency of 3 Hz [72, 73] (Figure 11)

2.5.3 Calculation rFE and rFD

For both datasets, the subjects have all executed three reference, three lengthening, and three shortening trials per condition. rFE and rFD were calculated as the percentual difference in torque between the reference and either the lengthening or shortening trial, with the corresponding condition (i.e. ankle angle or muscle). rFE was calculated with the following formula [41]:

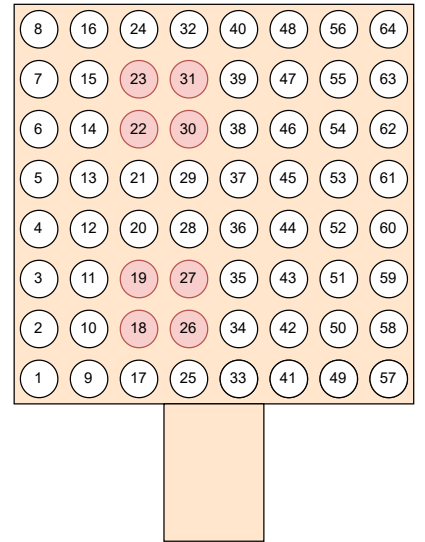$$rFE = \frac{\tau_{length} - \tau_{ref}}{\tau_{ref}} \cdot 100\%, \tag{9}$$
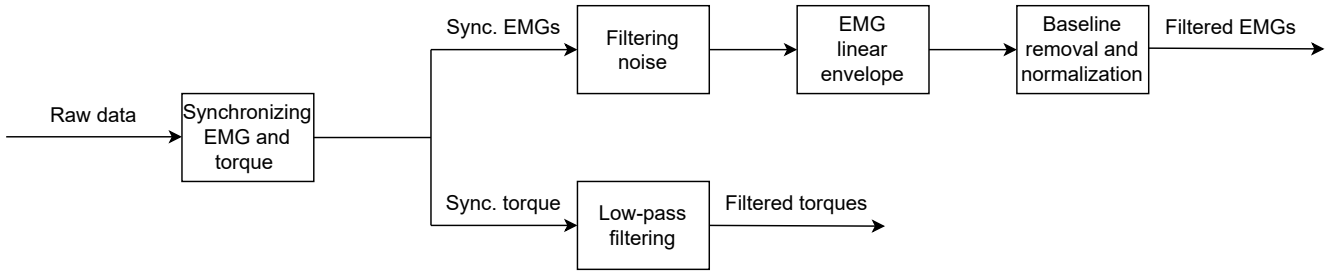
Figure 11: Schematic overview of the pre-processing of the data, i.e. the EMGs and the torques.

with τ_{length} the measured torque of the lengthening trial, and τ_{ref} the measured torque of the reference trial.

rFD was calculated with a similar formula as rFE:

$$rFD = \frac{\tau_{short} - \tau_{ref}}{\tau_{ref}} \cdot 100\%, \tag{10}$$

with τ_{short} the measured torque of the shortening trial. rFE and rFD were both calculated over the entire time range, i.e. the torque per time-step. This calculation was used to assess the trend of rFE and rFD. Additionally for quantifying both rFE and rFD, seven time windows were determined with a length of $0.5\,\mathrm{s}$ each. The windows that were chosen, were 2.5, 5.0, 7.5, 10.0, 12.5, 15.0, and $17.5\,\mathrm{s}$ after the transition, i.e. when the ankle angle changes. These calculations were used for assessing whether someone exhibits rFE and/or rFD.

2.6 Data evaluation

2.6.1 Selection of trials

Some articles choose 'the best trials' to present their results regarding the magnitude of rFE and rFD [20]. This means that often the combination of one lengthening, one shortening, and one reference trial is chosen which results in the highest rFE and rFD [74, 75]. In this research, a similar approach was used. Additionally, other parameters were also considered in the selection of the trials, specifically the activation level of the trials and the measured muscle activity of the other muscles. Ideally, the activation level is as similar as possible, as the torque generation is dependent on the muscle activity [76]. Also, co-contraction should be as small as possible for all trials, as co-contraction also affects the measured torque [77].

For the assessment of the activation level, the root mean square error (RMSE) was calculated for the activation level between the reference trial and either the lengthening or shortening trial. The RMSE was a measure to quantify the difference between two different values. The higher the value, the larger the error between the measured EMGs. The threshold was set on an error of $2\,\%$. In the case, that the RMSE was smaller than $2\,\%$, the activation levels of the different trials were considered equal and comparable.

Finally, the muscle activity of the four measured muscles was assessed. This was accomplished by calculating the mean of the normalized muscle activation. Ideally, the amount of co-contraction was as small as possible, such that the measured torque was mainly obtained by the measured muscle. If the muscle activation of the other three muscles, i.e. GL, GM, and either TA or SOL, was each smaller than $5\,\%$ then the trials were appropriate to use.

2.6.2 Statistical analysis

To analyze both the influence of the different muscle lengths and the different muscles, the calculated rFE and rFD of the entire time series were used. To take the time dependency into account, the data was analyzed by means of statistical parametric mapping (SPM) [78]. The SPM-based statistical testing was conducted on the entire dataset, which quantifies the probability of significant differences throughout the entire measurement with a specific test statistic value. By means of SPM a paired sample t-test was used for determining the influence of the muscle length and muscle itself on the magnitude of both rFE and rFD. The level of significance was set to $\alpha < 0.05$.

2.6.3 Classification of the trials

The determination of whether a subject exhibits rFE or rFD was determined by means of descriptive statistics. Per subject were the rFE and rFD per time window calculated and were included in boxplots per subject and condition.

The boxplots depicted how the rFE or rFD was distributed and if rFE or rFD was observed. If Q1 of the boxplot, which is the median of the first half of the data points (at 25 %), was higher than zero for the lengthening trials, then the measured difference in torque was classified as rFE. If Q3, which is the median of the second half of the data points (at 75 %), was lower than zero for the shortening trials, then the trial was classified as rFD. In any other case, the trial was labeled as no observed rFE or rFD.

2.6.4 Classifier

As mentioned, the classifier requires training data and test data. The training data was for the model to calculate the prediction and/or likelihood of the occurrence of rFE given some input parameters. For increasing the training dataset, all three repetitions of the lengthening trials were assessed and classified in combination with one reference trial per subject, specifically the reference trial that was previously chosen in Section 2.6.1.

The first input parameter was the classification of whether rFE was exhibited or not when measuring on the TA. This was done in the same manner as explained in Section 2.6.3. The other input parameters were the normalized mean activation level of the lengthening trial, the variance in activation level of the lengthening trial, the stretch amplitude, the normalized ankle angle, and the differences in the mean of the activation levels of the reference trial and the lengthening trial. The normalized ankle angle was a value between 0 and 1, with 0 being the angle that produced the smallest torque and 1 being the angle that produced the highest torque.

By means of the Classification Learner app on Matlab, multiple classification models were trained and validated. This tool provides the opportunity to assess the performance of different models in the search for the most appropriate model for the input data and the predetermined classifications. The model types that were assessed, were Linear Discriminant Analysis (LDA), Quadratic Discriminant Analysis (QDA), Logistic Regression (LR), Support Vector Machine (SVM), K-Nearest Neighbor (KNN), and Gaussian Naïve Bayes (GNB). This Matlab app generates predictions as the response based on new data, which was cross-validated five times. After the assessment of the models, which was described in Section 2.6.5, the input data was varied by excluding one of the five input variables one by one.

2.6.5 Classifier assessment

The selected classification models were evaluated on their ability to predict the occurrence of rFE on the TA correctly. The evaluation was based on the accuracy, precision, specificity, recall, and the f_1 score, in correspondence with the research of Pascual-Valdunciel *et al.* (2022) [65] to assess the classification models. The metrics were determined by means of true positives (TP), false positives (FP), true negatives (TN), and false negatives (FN).

The equations are as follows [65]:
$$Accuracy = \frac{TP + TN}{TP + FP + TN + FN}, \tag{11}$$

where accuracy is a measure for assessing how many predictions are correct.

$$Precision = \frac{TP}{TP + FP}, \tag{12}$$

where precision is a measure for assessing how many of the positive predictions are correct.

$$Specificity = \frac{TN}{TN + FP}, \tag{13}$$

where specificity is a measure for assessing how many of the actual negative classifications are predicted correctly.

$$Recall = \frac{TP}{TP + FN}, \tag{14}$$

where recall is a measure for assessing how many of the actual positive classifications are predicted correctly.

$$f_1 = 2 \cdot \frac{Precision \cdot Recall}{Precision + Recall}, \tag{15}$$

where the f_1 score summarizes the performance of the model based on both the negative and the positive predictions. For all metrics, the score ranges between 0 and 1, with 1 being the score indicating the best possible performance.

3 Results

3.1 rFE and rFD

The results in terms of quantification of the history-dependent muscle properties are presented first. The selected trials can be found in Appendix B. To quantify both rFE and rFD, the results are presented separately for each dataset as the mean rFE and rFD across all subjects for the entire measurement period and the mean rFE and rFD per time window.

3.1.1 Dataset A - Operating region

The results of dataset A are presented in Figure 12 and Table 2. Both provide an overview of the average rFE and rFD measurements across all subjects. Concerning the rFE measurements, both the rFE measured on the ascending limb and on the plateau region approached zero over time. Additionally, it is noteworthy that the rFE measured on the plateau region was consistently higher than the rFE measured on the ascending limb region with an average difference of $3.98 \pm 1.20\,\%$. However, the statistical analysis did not reveal a significant difference between the magnitude of these two operating regions within the force-length relationship.

Considering the results of the rFD measurements, the values remained consistent over time for both regions within the force-length relationship. Particularly up to the third time window, at $7.5\,\mathrm{s}$, the rFD for both regions were of similar magnitude. However, after the third time window, the rFD of the plateau region became less negative compared to the rFD of the ascending limb. On average, the rFD of the ascending limb was greater than the plateau region, with a mean difference of $2.22 \pm 1.96\,\%$. Again, the statistical tests did not reveal a significant difference between the magnitude of the two operating regions within the force-length relationship.

Table 2: The average rFE and rFD across subjects per time window of dataset A.

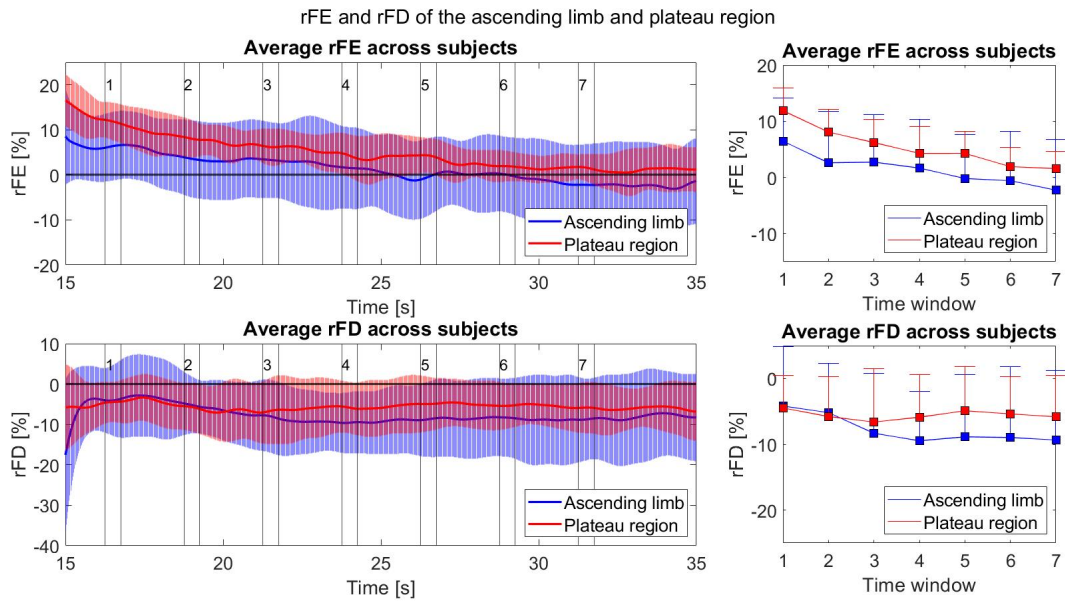|		Time window						
		1	2	3	4	5	6	7
rFE	AL	6.47 ± 7.65	2.56 ± 9.24	2.70 ± 8.47	1.64 ± 8.66	-0.18 ± 7.77	-0.60 ± 8.72	-2.28 ± 9.02
(% ± STD)	PR	11.85 ± 4.11	8.06 ± 4.09	6.23 ± 4.05	4.26 ± 4.76	4.26 ± 3.92	1.92 ± 3.37	1.54 ± 3.02
rFD	AL	-4.19 ± 8.99	-5.17 ± 7.47	-8.30 ± 9.06	-9.48 ± 7.50	-8.88 ± 9.50	-8.98 ± 10.76	-9.34 ± 10.51
(% ± STD)	PR	-4.48 ± 5.00	-5.74 ± 6.04	-6.62 ± 8.16	-5.85 ± 6.39	-4.91 ± 6.72	-5.36 ± 5.65	-5.36 ± 6.27

Figure 12: The mean and STD of each condition, i.e. operating muscle length, regarding both rFE and rFD. The blue line represents the ascending limb region and the red line represents the plateau region. The error bars are in all four figures the STD.

The scatterplots (Figure 13) show the relation between the activation level of the lengthening and shortening trial with the average rFE and rFD of dataset A throughout the entire time series. In general, the average activation level measured on the plateau region was higher compared to the measurements on the ascending limb for both the rFE and the rFD measurements. However, visually no clear difference can be seen in the magnitude of rFE with respect to the activation level. The rFD measured on the plateau region was closer to zero compared to the ascending limb measurements. The top figure on the right-hand side of Figure 13 shows a slight increase in rFE with increasing differences in activation level, whereas a positive difference indicates a higher activation level of the lengthening trial with respect to the reference trial. Regardless of the differences in activation level, the magnitude of rFE was consistently larger than zero when measured on the plateau region. The spread of the magnitude of rFE was larger when measured on the ascending limb. With respect to the bottom figure, no clear visual difference can be found with respect to the differences in activation level.
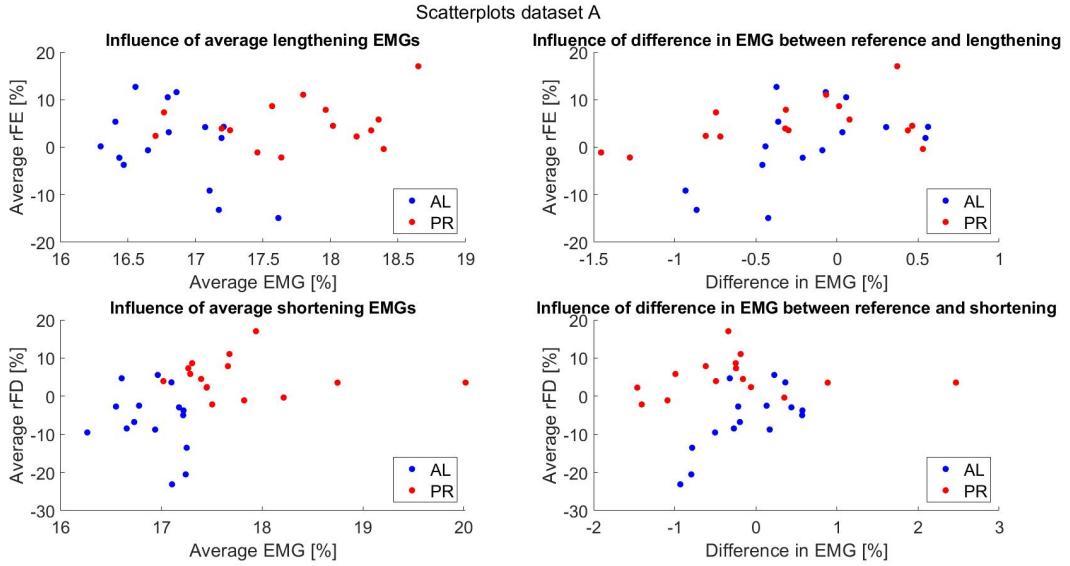

Figure 13: Scatterplots for assessing the influence of the muscle activation level with respect to the measured rFE and rFD of dataset A. All lengthening and shortening trials are considered with respect to one of the reference trials per subject leading to six combinations per subject per condition. A negative difference in EMGs indicates a higher average EMG of the reference trial compared to either the lengthening or shortening trial.

3.1.2 Dataset B - Fiber types

The results of dataset B, designed for assessing the influence of different fiber type compositions on the magnitude of rFE and rFD, are presented in Figure 14 and Table 3. Considering the rFE measurements, the TA measurements had a similar pattern as dataset A where the rFE decreased over time. The rFE of the SOL measurements, on the other hand, increased gradually until approximately the third time window. After this increase, the measured rFE also showed a decreasing trend over time. The TA measurements were consistently higher than the SOL measurements with an average difference of $4.73 \pm 4.67\,\%$. The performed statistical analysis did not result in a significant difference between the two muscles.

It was evident that the rFD of the SOL exhibited more fluctuations than the rFD of the TA. However, the rFD measurements were both relatively consistent over time in terms of the average magnitude. The rFD of the measurements of the TA is only $1.69 \pm 2.09\,\%$ greater in magnitude than the SOL measurements. The statistical tests did not yield any significant difference between the rFD of both muscles.

Table 3: The average rFE and rFD per time window of dataset B.

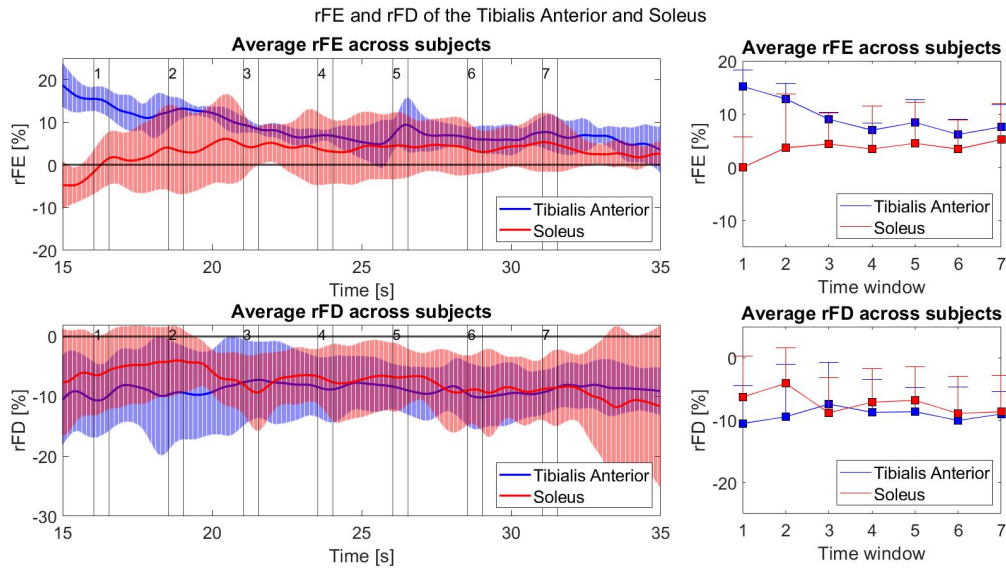|		Time windows						
		1	2	3	4	5	6	7
rFE	TA	13.94 ± 5.50	11.59 ± 3.60	7.83 ± 3.75	5.74 ± 2.60	7.21 ± 7.77	4.93 ± 2.82	6.36 ± 4.56
(% ± STD)	SOL	-0.04 ± 5.72	3.63 ± 10.09	4.37 ± 5.88	3.43 ± 8.04	4.51 ± 7.71	3.39 ± 5.49	5.21 ± 6.77
rFD	TA	-11.59 ± 4.88	-10.60 ± 7.02	-8.60 ± 4.83	-9.88 ± 3.12	-9.77 ± 2.03	-11.12 ± 3.96	-10.12 ± 1.47
(% ± STD)	SOL	-7.96 ± 4.81	-5.71 ± 4.62	-10.10 ± 3.79	-8.57 ± 4.56	-8.06 ± 4.80	-9.67 ± 5.44	-9.77 ± 5.20

Figure 14: The mean and STD of each condition, i.e. the different muscles, regarding both rFE and rFD. The blue line represents the TA measurements and the red line represents the SOL measurements. The error bars are in all four figures the STD.

The scatterplots (Figure 15) show the relation between the activation level of the lengthening and shortening trial with the average rFE and rFD of dataset B throughout the entire time series. The average activation level has a higher magnitude measured on the TA compared to the SOL. However, no clear visual difference in the magnitude of the rFE between the two muscles. The magnitude of rFD measured on the TA is more negative than the SOL. The scatterplots showing the relation between the differences in the activation level and the magnitude of the rFE and rFD do not show clear differences. However, the rFE measured on the TA is more consistently measured above zero compared to the SOL measurements regardless of the differences in EMG.
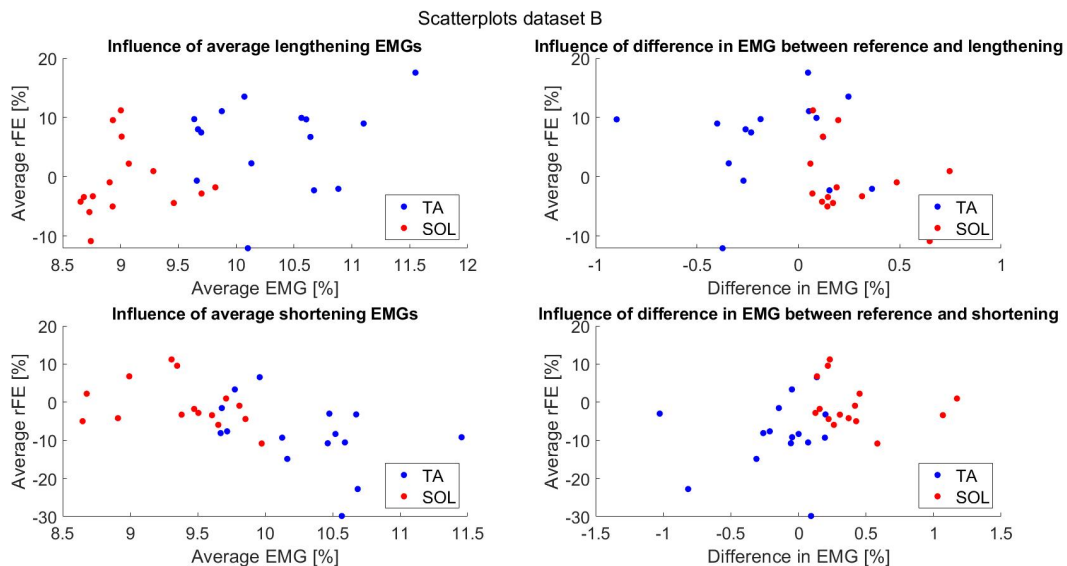

Figure 15: Scatterplots for assessing the influence of the muscle activation level with respect to the measured rFE and rFD of dataset B. All lengthening and shortening trials are considered with respect to one of the reference trials per subject leading to six combinations per subject per condition. A negative difference in EMGs indicates a higher average EMG of the reference trial compared to either the lengthening or shortening trial.

3.2 Classification of training data

Regarding dataset A (Figure 16), only subjects 3 and 4 exhibited rFE when measuring on the ascending limb region. For the plateau region, however, subject 2 was the only subject that did not exhibit rFE in that region. For classifying the data for rFD, only subject 1 on the ascending limb and subject 3 on the plateau region were classified as trials without rFD.
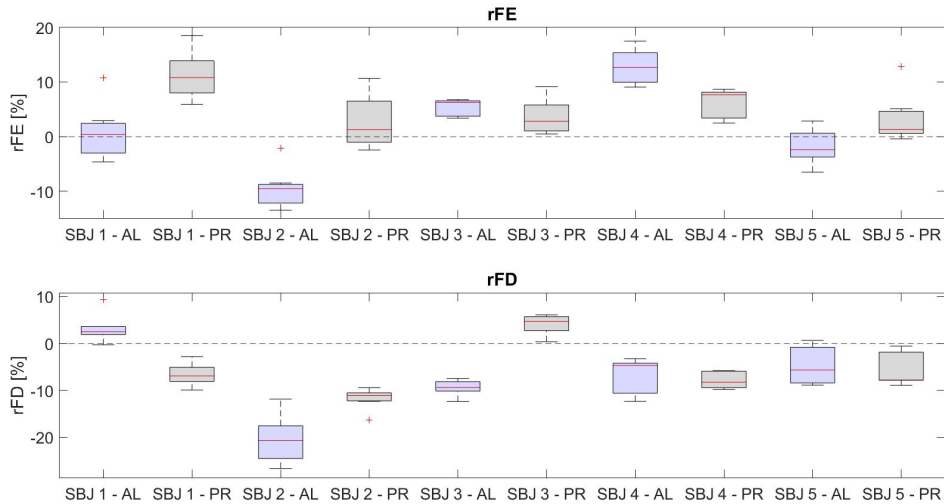

Figure 16: Boxplots of dataset A for the determination of whether rFE and rFD are exhibited per subject. The blue boxplots represent the data measured on the ascending limb region. The grey boxplots represent the data measured on the plateau region.

For dataset B (Figure 17), the same was done regarding the classification of the trials. While all subjects exhibited rFE when measuring on the TA, rFE was not observed for all subjects when measuring on the SOL, specifically subject 2, subject 3, and subject 5. For classifying rFD, only subject 2 on the SOL and subject 4 on the TA did not exhibit rFD.
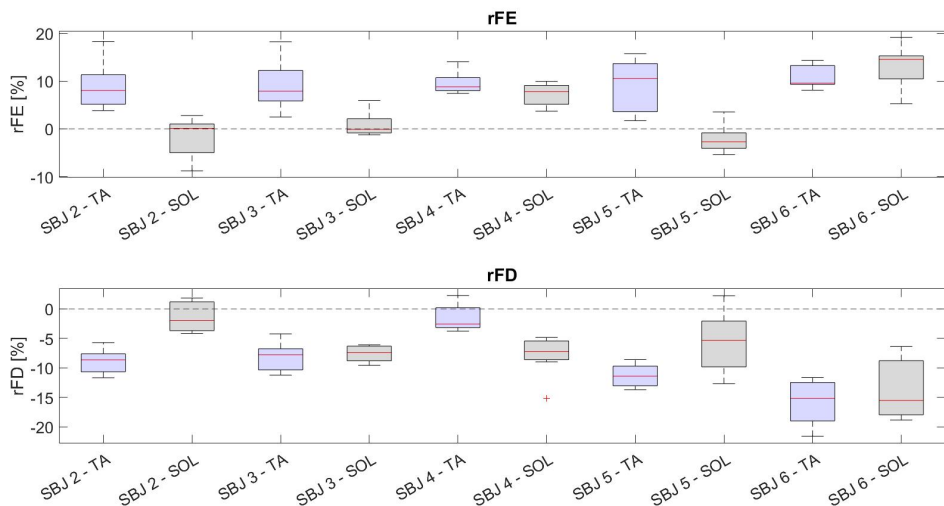

Figure 17: Boxplots of dataset B for the determination of whether rFE and rFD are exhibited per subject. The blue boxplots represent the data measured on the tibialis anterior. The grey boxplots represent the data measured on the soleus.

3.3 Machine learning classifier

For the assessment of the classification technique, the data of the rFE measurements of the TA were utilized regardless of dataset and condition, i.e. operating region of force-length relationship and activation level. This dataset included all lengthening trials, each paired with one reference trial per subject, resulting in a total of 45 combinations of trials - comprising 30 of dataset A and 15 of dataset B. In some trials of the dataset, no rFE was observed while in other trials, even of the same subject, rFE was observed. In total, rFE was observed in 28 trials.

Figure 18 summarizes the classification results when using all variables as described in Section 2.6.4. When comparing all classification techniques, GNB scored consistently lower than the other algorithms while having scores of less than 0.65. On the other hand, the machine learning classifiers of the LDA and LR yielded the highest scores, each surpassing 0.70. Both LDA and LR obtained the highest scores for all metrics (Accuracy = 0.78, Precision = 0.82, Specificity = 0.71, Recall = 0.82). The SVM algorithm also demonstrated good performance, with scores slightly lower than those of LDA and LR. with an average 0.025 ± 0.015 smaller considering all metrics.

Additionally, considering the f_1 score of these algorithms, which provides an overall assessment of the classifier performance, the scores of both LDA and LR were 0.82. The SVM classifier obtained an f_1 score of exactly 0.80. The other classifiers had lower values for the validity metrics. Consequently, only LDA, LR, and SVM were considered for assessing the influence of the different input variables on the performance of the predicting models.
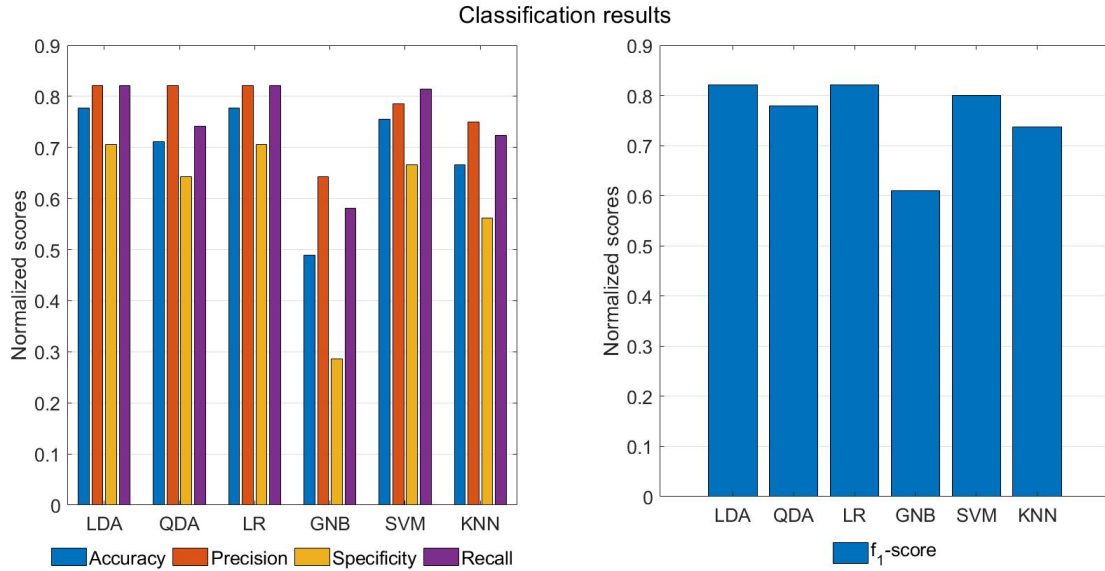

Figure 18: Classification results of the validation metrics: accuracy, precision, specificity, recall, and f_1 score. The training data consisted of all input variables.

To compare the performance of the three machine learning algorithms while excluding one input parameter at a time, only the f_1 score was considered. Considering the results of Figure 19, excluding the variables related to the muscle activation level resulted in a lower overall performance of the classifier compared to the classifier when all input parameters were used. Excluding the variable representing the average activation level of the lengthening trial led to a performance reduction of $12.9 \pm 1.3\%$. Similarly, the variance of the activation level of the lengthening resulted in a decrease of $3.8 \pm 0.9\%$, and the difference in activation level between the reference and lengthening trial led to a decrease of $6.2 \pm 1.2\%$. However, when considering the stretch amplitude, the exclusion of this variable did significantly impact the performance of any classifier.

Finally, the normalized ankle angle resulted in a distinct outcome for all three classifiers. The LDA and SVM algorithms showed minor differences in performance, -1.4% and 0.7% respectively, when this variable was excluded. The LR classifier, on the other hand, showed a decrease of 8.8% in performance when the normalized ankle angle was omitted from the dataset.
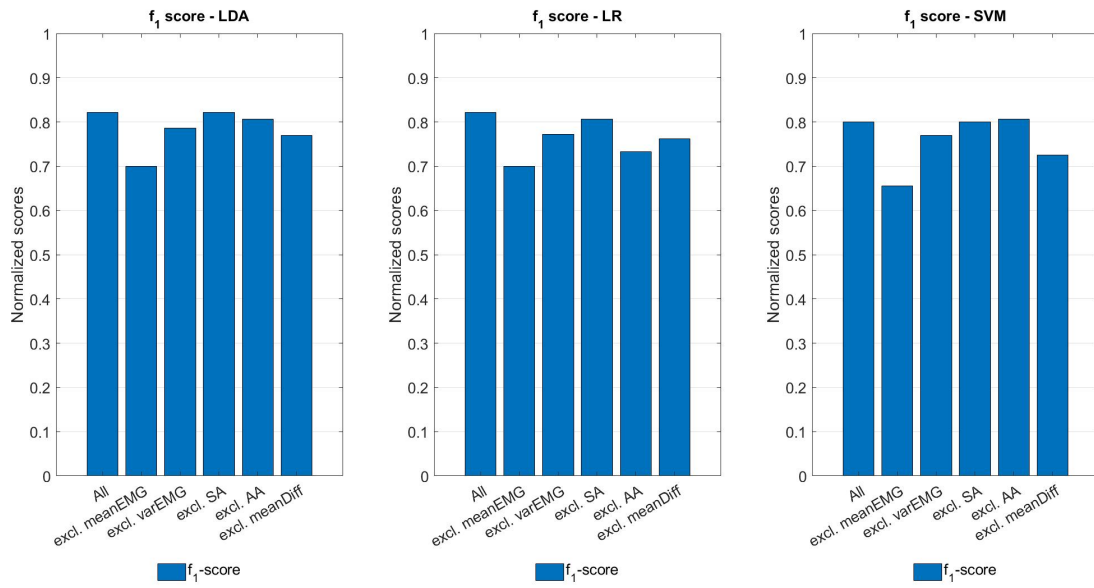
Figure 19: f_1 scores for the classifiers that scored the highest, i.e. LDA, LR, and SVM. The first bar (of all three plots) represents the f_1 score of the classifiers when all input variables are used. The second to the sixth bar excludes each time one input variable, excluding the mean normalized activation level (meanEMG), the variance of the normalized activation level (varEMG), the stretch amplitude (SA), the normalized ankle angle (AA), and the mean difference in activation level of the reference and lengthening trial (diffEMG), respectively.

4 Discussion

This study consisted of two main parts. The first part aimed to quantify the magnitude of rFE and rFD to investigate the influence of the muscle's operating region on the force-length relationship (dataset A) and the muscle fiber type distribution (dataset B). The second part aimed to predict the occurrence of rFE measured on the TA by means of machine learning algorithms.

It was hypothesized that the operating region and the muscle-fiber type distribution do influence the magnitude and occurrence of rFE, but not of rFD. It is expected that the rFE is better captured in the plateau region and when measuring on muscles with a relatively higher proportion of type II fibers compared to type I fibers. However, when measuring for rFD, it is hypothesized that no differences between the two conditions would be observed.

4.1 Influence of the operating region

To quantify the magnitude of rFE when measuring different regions of the force-length relationship, the magnitude of the rFE approached zero over time, although the rFE of the plateau region consistently exceeded that of the ascending limb region with $3.98 \pm 1.20\,\%$. Regarding the measured rFD, both regions exhibited a similar and constant torque reduction regardless of time. On average, the ascending limb exhibited a higher rFD with $2.22 \pm 1.96\,\%$. However, statistical significance was not found for any conditions or time window. This outcome is in agreement with the hypothesis regarding the rFD, but contradicts the expectations regarding rFE.

The absence of statistical significance in the findings is likely attributable to the considerable variance within this dataset. The dataset is inconsistent in terms of stretch amplitude (Table 1), a known variable influencing the magnitude of rFE and rFD [11, 39]. Additionally, voluntary contractions introduce variability, as subjects may not consistently maintain the required activation level. During submaximal voluntary contractions, subjects have the ability to compensate using antagonist muscles, thereby influencing the measured ankle torque even if the instructed activation level is ostensibly achieved. This resulted in intra-individual variances in terms of activation level and measured torque. Also, a large inter-individual difference in terms of rFE and rFD was present as the torque showed high variability under the same conditions (Appendix C). These factors likely contributed to the lack of statistical significance in the results.

The classification of the subjects into responders and non-responders was done by means of boxplots (Figure 16 and 17). Using this method, two of the five subjects were classified as responders for exhibiting rFE when measuring in the ascending limb region. On the contrary, four of the five subjects are categorized as responders for exhibiting rFE when measuring in the plateau region. Even though the rFE of subject 3 and 4 is lower for the plateau region compared to the ascending limb region, this outcome suggests that rFE might be better captured in the plateau region. Therefore, the operating muscle's length still might influence the magnitude and occurrence of rFE, despite the statistically insignificant results across all subjects. The classification of responders and non-responders on the rFD measurements did not reveal large differences between the two operating muscle regions. The outcome of the classification and calculated average across subjects support the hypothesis that the force-length relationship does not influence the occurrence and magnitude of rFD.

In previous studies, the measured rFE obtained in similar measurements had the magnitude between the 4-25 % when measuring on dorsi- and plantar flexors [45, 75, 79–83]. The average values of the ascending limb region and plateau region are in accordance with previous studies. Notable is that the found values of this study are relatively low compared to the literature. However, the difference in magnitude can be explained by the chosen time windows of the study. As the results showed, the rFE decreased over time, indicating that selecting a time window during the transition of ankle angle results in a higher rFE compared to a time window after this transition. The further the time window is from the transition, the smaller the obtained rFE. The rFD that is measured in previous studies had the magnitude of 9-39 % when measuring on dorsi- and plantar flexors [43, 44, 84, 85]. The measured rFD of this study is smaller in magnitude than found in these previous studies.

The selection of trials is a crucial aspect of calculating the rFE and rFD. As mentioned, some studies select the trials that result in the highest difference in torque [74, 75, 82] and others remove the non-responders from the dataset [80]. Both actions result in rFE and rFD that are positively biased [20]. Previous studies also vary in the criteria regarding the activation level. The scatterplots of Figure 13 and 15 indicated that there might be a relation between the difference in muscle activation level and the magnitude of rFE. This requires, however, confirmation of future research with a greater number of subjects. Ideally, the EMG profile and mean of the selected trials are as similar as possible to exclude this possibility. Therefore, the RMSE of the normalized activation level is included in the selection of the trials for this study. As both rFE and rFD are considered per subject, choosing the trials

resulting in the highest rFE might be the combination that results in a smaller rFD. Notable, the selection of the best trials leads to positively biased results. In this study, a combination of a low RMSE and the highest rFE or lowest rFD has been used for the selection of the trials. However, this also resulted in relatively lower rFE and rFD compared to the literature.

4.2 Influence of muscle fiber composition

The rFE measurement, of dataset B, on the TA shows a similar trend as the measurements of dataset A, starting with an increasing torque and then decreasing torque over time. The rFE measurements on the SOL, first show an increase in rFE and afterwards slightly following the trend of the TA measurements. The TA measurements were on average $4.73 \pm 4.67\%$ higher than the SOL measurements. The rFD measurements of both muscles showed consistent torque reduction regardless of time. On average, the ascending limb exhibited a higher rFD with $1.69 \pm 2.09\%$. For both rFE and rFD, there was no statistical difference between the two muscles. This outcome supports the hypothesis regarding the rFD but contradicts the hypothesis of the rFE.

The increase in rFE shortly after the transition of the SOL measurements was due to the challenge of maintaining the activation level during plantar flexion. All subjects dropped in activation level after the transition, after which it took some time to reach the target activation level again. Consequently, this resulted in a drop in measured torque, which could explain the difference in rFE for the TA and the SOL. Regardless of this difference, statistical significance was not found. Similar to the measurements of dataset A, both rFE and rFD across the subjects of dataset B show a high variability resulting in a large spread of the data. As mentioned in Section 4.1, the submaximal voluntary contraction results in high variation. Additionally, the activation level of 7.5-12.5%MVC is lower than reported in the literature which makes comparing results challenging. Comparing the values of the rFE and rFD of both the TA and the SOL, all values are in agreement with the literature but are relatively low [45, 75, 79–83, 86–88]. As mentioned in Section 4.1, the magnitude of the obtained rFE and rFD are dependent on the selection of the trials and the selection of the time window.

The classification of the subjects categorized the subjects into the classes responders or non-responders. When measuring the TA, all subjects exhibited rFE, while for the SOL only two subjects exhibited rFE. For both the TA and the SOL, four of the five subjects exhibited rFD. These results indicate that the rFE when measuring on the TA is better captured compared to the SOL. However, the measurements on the SOL did not exclude that other factors are contributing to the measured torque. The experiments when measuring the SOL resulted in discomfort for the subject due to the footplate pressing the posterior side of the ankle. Consequently, the subjects lifted their heel which resulted that the ankle was not aligned with the Achilles motor. Additionally, it required much effort to reach the target activation level of the SOL. The high effort of the SOL trials might be due to the different knee angles while measuring the history-dependent properties and the MVC trial. Having a more flexed knee, the activation level of the soleus is smaller compared to when the knee is extended [87]. Additionally, the subjects are instructed to reach the target activation level of 7.5-12.5%MVC, which might be challenging to capture in the presence of noise.

Comparing two different muscles *in vivo* requires generalizability. Importantly, the subjects were measured in the same configuration in order to be consistent with the influence of posture and joint angles. Moreover, the EMGs were normalized by means of an MVC trial for obtaining comparable EMG amplitudes. Ideally, the MVC of both the TA and the SOL were measured in the same configuration to exclude the influence of different joint angles on the normalized EMG amplitudes [89]. However, the amount of force produced by different muscles can vary, whereas force production also varies with different joint configurations. Generalizability could be improved by measuring the MVC in the same configuration as the history-dependent measurements. This ensures the functional MVC is measured for the joint configuration of the experiments, leading to a more accurate normalization of the MVC.

Ankle torque is primarily generated by the TA when dorsiflexing. Regarding the SOL measurements, however, the gastrocnemeii are also contributing to the ankle torque while plantar flexing. During the trials, the knee angle was 100-110° to minimize the effect of the gastrocnemeii on the ankle torque [90]. However, the gastrocnemeii are still activated despite the flexed knee angle and still contribute to the plantar force production [87]. Additionally, the influence of the gastrocnemeii on the plantar force production might have influenced the ankle-torque relationship, as the gastrocnemeii are operating in the ascending limb region [91]. Within the ROM of the ankle, the plateau region could not be distinguished from this curve (Appendix A). An explanation could be, is that no plateau is found as both the gastrocnemeii and the SOL are measured simultaneously or because the SOL is merely operating at the ascending limb [92]. Furthermore, the fiber-type distribution of both the TA and SOL are based on values found in the literature. The exact composition of muscle fibers is subject-specific [9]. Due to the contribution of the gastrocnemeii on the ankle torque, and the uncertainty regarding fiber-type composition and the operating region of

the force-length relationships, no firm conclusion can be drawn from this experiment with regard to the influence of fiber-type composition on the history-dependent properties.

4.3   Machine learning classifier

This study assessed the feasibility of using machine learning techniques to predict the occurrence of rFE on the TA based on EMG- and kinetic data. The machine learning models were trained and validated in order to categorize the input data into the *rFE* or *no rFE* classes. Six models were assessed of which only three models, i.e. LDA, LR, and SVM, showed high classification performance with an f_1 score of 0.8 or higher [65]. The difference between the f_1 of the three classifiers was subtle. The highest assessment metrics were found for the precision and recall of 0.82 for both the LDA and LR, indicating good performance in classifying the positive values into the *rFE* class. The data that belongs to the *no rFE* class are predicted less accurately, where the specificity is highest for LDA and LR with a value of 0.71. The results indicate that rFE on the TA can be predicted to some extent. The results of the classifier can not be compared to the literature as the performance of the model is dependent on the dataset and to our knowledge, no other machine learning model is used for predicting history-dependent muscle properties.

The input parameters of the classification models have been altered to investigate the parameters that influence the occurrence of rFE. The parameter that resulted in the largest decrease of the f_1 score for all three classifiers was the average activation level of the lengthening trials, followed by the difference in activation level between the reference and lengthening trials and the variance of the activation level. This outcome suggests that the activation level is an important factor in the occurrence of rFE. However, the exclusion of the variance of the EMGs and the differences between the EMGs also indicates that the differences in activation level are also affecting the outcome and the occurrence of rFE. Additionally, the selection of the trials is also affecting the detection of this muscle property. The stretch amplitude did not result in any difference in model performance. However, the stretch amplitude was a constant value of 7.5° with the exception of 6 of the 45 trials, which was 15°. The stretch amplitude should have varied in order to draw firm conclusions on the influence of this variable on rFE. The normalized ankle angle, however, did not yield clear results as specifically the LR model suggests that the ankle angle, and therefore the operating region of the force-length relationship, is influencing the occurrence.

4.4   Limitations and future work

In general, *in vivo* measurements for assessing muscle properties have their limitations due to the complexity of the human body. Despite these limitations, this research conducted measurements to investigate the influence of the operating region of the muscle and of the muscle fiber composition. Regarding both experiments, the selection of trials is critical as it strongly affects the outcome of the research. In agreement with other articles, this research selected 'the best trials' in combination with the evaluation of the muscle activation level in order to compare results with the literature. Consequently, the results are biased to positive values [20].

For future work, it is recommended to have a general approach for assessing the results, specifically the muscle activation level. It is suggested to select the most suitable trials merely based on the similarities in activation level. In accordance with the Consensus for Experimental Design of Electromyography (CEDE) project, the activation level can be evaluated by considering the root mean square (RMS) value [93]. The trials with the highest similarities in EMGs, with regard to all muscles influencing the measured joint torque, should be considered for the calculation of history-dependent muscle properties. It is not suggested to choose trials that lead to the highest rFE or the lowest rFD, as this gives positively biased results. Additionally, the MVC trial should be as similar as possible as it influences the normalization process. According to the CEDE project, the preferred method is to perform an MVC trial which corresponds with the task performed during the experiments, if possible, since it represents the true MVC in the context of the experiments. However, a normalization by means of a standardized isometric MVC trial, which does not correspond with the task performed during the experiments, is also suitable to use for comparing the same muscle and different muscles within the same subject [89].

Another limiting factor of the study is the design of the SOL experiments, as discussed in Section 4.2. Ideally, the ROM of the ankle is less restricted. Therefore, it is recommended to adjust to footplate by lowering the plate located at the heel. Another recommendation is the adjustment of the MVC trials in order to maintain the same joint configurations as the history-dependent trials such that reaching the target level is less challenging. The uncertainty of the muscle fiber type distribution is also limiting the reliability of the research. By means of the decomposition of HD-EMG signals, the subject-specific fiber type can be estimated [93]. This requires an additional trial, in which the subject is instructed to perform contractions at multiple different submaximal voluntary contractions. First, the

contraction is linearly increasing from rest to the target activation level followed by a constant force production at the target activation level [94].

The overall performance of machine learning classifiers is strongly dependent on the dataset itself, and the dataset is in this research also the limiting factor. Small datasets contain fewer details, which results in an unreliable and biased model [95]. Therefore, increasing the size of the dataset could lead to a better performance of the classifiers. Moreover, the predicting parameters are essential for increasing the model's performance. Therefore, feature selection is a method to remove irrelevant parameters from the input variables, leading to less computation time and increased learning accuracy [96]. Additionally, this method is useful for obtaining insight into which parameters are influencing the occurrence of rFE *in vivo*. The used algorithm should suit the dataset and is, therefore, also affecting the overall performance of the model. Choosing the most appropriate dataset also depends on the dataset and is often chosen by evaluating multiple models with the assessed dataset [97].

5 Conclusion

In this research, the influence on the operating region of the force-length relationship and of the muscle fiber type composition of muscles on the magnitude of history-dependent muscle properties, i.e. rFE and rFD, are quantified. Moreover, machine learning classifiers are evaluated on their ability to predict the occurrence of rFE when measured on the TA.

The obtained rFE was on average higher at the plateau region compared to the ascending limb, while the rFD measured on the ascending limb was larger in magnitude. Categorizing the individual subjects resulted in more responders for rFE at the plateau region and no clear difference for rFD. Despite the absence of statistical significance, the results still suggest that a relationship between the operating region and the occurrence of rFE might exist. This requires future research with a dataset containing less inter-individual variance or a larger dataset. Regarding rFD, no relation is found with the operating region of the muscle.

Similarly, the rFE measured on the TA was higher in magnitude than the SOL, and more subjects were categorized as responders. The dataset contained a high variance and the experiments did not exclude the effect of other factors influencing the measured torque sufficiently. Therefore, the relation between muscle fiber type composition and rFE should be investigated in future work. Again, no relation is found between rFD and muscle fiber type.

Finally, the results of the classification models suggest that rFE can be predicted, especially by means of muscle activation data. The models that showed the best results are LDA, LR, and SVM. However, this is strongly dependent on the available dataset, indicating that for other data a different machine learning technique might provide a better classification.

Several aspects of these history-dependent muscle properties remain not fully understood. Applying the approach presented in this thesis in future research could be used to better establish the influencing parameters on the occurrence and magnitude of the history-dependent muscle properties. The use of machine learning algorithms could provide useful insights into the influence of EMG- and kinetic-related properties on rFE and rFD. These properties could be integrated into EMG-drive musculoskeletal models, providing more accurate models with respect to daily human movement. Further research is required to verify its relevance in daily living, the underlying mechanisms, and the influencing parameters of these history-dependent muscle properties.

References

[1] A. Godfrey et al. "Direct measurement of human movement by accelerometry". In: *Medical Engineering and Physics* 30.10 (2008), pp. 1364–1386. ISSN: 13504533. DOI: 10.1016/j.medengphy.2008.09.005.

[2] Walter R. Frontera and Julien Ochala. "Skeletal Muscle: A Brief Review of Structure and Function". In: *Behavior Genetics* 45.2 (2015), pp. 183–195. ISSN: 15733297. DOI: 10.1007/s00223-014-9915-y.

[3] Bernardo Innocenti. "Biomechanics: A fundamental tool with a long history (and even longer future!)" In: *Muscles, Ligaments and Tendons Journal* 7.4 (2017), pp. 491–492. ISSN: 22404554. DOI: 10.11138/mltj/2017.7.4.491.

[4] Christian Cajavilca, Joseph Varon and George L. Sternbach. "Luigi Galvani and the foundations of electrophysiology". In: *Resuscitation* 80.2 (2009), pp. 159–162. ISSN: 03009572. DOI: 10.1016/j.resuscitation.2008.09.020.

[5] Elaine N. Marieb and Katja Hoehn. *Human Anatomy and Physiology*. Tenth. Pearson, 2016. ISBN: 978-1-292-09697-1.

[6] A F HUXLEY. "Muscle structure and theories of contraction." eng. In: *Progress in biophysics and biophysical chemistry* 7 (1957), pp. 255–318. ISSN: 0096-4174 (Print).

[7] Jenna A. Monroy et al. "What is the role of titin in active muscle?" In: *Exercise and Sport Sciences Reviews* 40.2 (2012), pp. 73–78. ISSN: 00916331. DOI: 10.1097/JES.0b013e31824580c6.

[8] Thomas K Uchida and Scott L Delp. *Biomechanics of Movement : The Science of Sports, Robotics, and Rehabilitation*. English. The MIT Press. Cambridge, Massachusetts: The MIT Press, 2020. ISBN: 9780262044202. URL: http://ezproxy2.utwente.nl/login?url=https://search.ebscohost.com/login.aspx?direct=true&db=nlebk&AN=2371099&site=ehost-live.

[9] W L Kenney, J H Wilmore and D L Costill. *Physiology of Sport and Exercise*. Human Kinetics, 2021. ISBN: 9781718201736. URL: https://books.google.nl/books?id=pIYhEAAAQBAJ.

[10] Lucas G. Prado et al. "Isoform diversity of giant proteins in relation to passive and active contractile properties of rabbit skeletal muscles". In: *Journal of General Physiology* 126.5 (2005), pp. 461–480. ISSN: 00221295. DOI: 10.1085/jgp.200509364.

[11] Wolfgang Seiberl, Geoffrey A. Power and Daniel Hahn. "Residual force enhancement in humans: Current evidence and unresolved issues". In: *Journal of Electromyography and Kinesiology* 25.4 (2015), pp. 571–580. ISSN: 18735711. DOI: 10.1016/j.jelekin.2015.04.011. URL: http://dx.doi.org/10.1016/j.jelekin.2015.04.011.

[12] A.M. Gordon, A.F. Huxley and F.J. Julian. "The variation in isometric tension with sarcomere". In: *The Journal of Physiology* 184 (1966), pp. 170–192. URL: http://e.guigon.free.fr/rsc/article/GordonAMEtAl66a.pdf.

[13] Fábio Carderelli Minozzo and Claudio Andre Barbosa de Lira. "Muscle residual force enhancement: A brief review". In: *Clinics* 68.2 (2013), pp. 269–274. ISSN: 18075932. DOI: 10.6061/clinics/2013(02)R01.

[14] W. Herzog, E.J. Lee and E. Rassier. "Residual force enhancement in skeletal muscle". In: *J Physiol* 574.3 (2006), pp. 635–642. DOI: 10.1113/jphysiol.2006.107748.

[15] Wolfgang A. Linke et al. "PEVK domain of titin: An entropic spring with actin-binding properties". In: *Journal of Structural Biology* 137.1-2 (2002), pp. 194–205. ISSN: 10478477. DOI: 10.1006/jsbi.2002.4468.

[16] Kiisa Nishikawa et al. "Calcium-dependent titin–thin filament interactions in muscle: observations and theory". In: *Journal of Muscle Research and Cell Motility* 41.1 (2020), pp. 125–139. ISSN: 15732657. DOI: 10.1007/s10974-019-09540-y. URL: https://doi.org/10.1007/s10974-019-09540-y.

[17] A. Mehta and W. Herzog. "Cross-bridge induced force enhancement?" In: *Journal of Biomechanics* 41.7 (2008), pp. 1611–1615. ISSN: 00219290. DOI: 10.1016/j.jbiomech.2008.02.010.

[18] Jackey Chen, Daniel Hahn and Geoffrey A. Power. "Shortening-induced residual force depression in humans". In: *J Appl Physiol* 126 (2019), pp. 1066–1073. DOI: 10.1152/japplphysiol.00931.2018.

[19] Atsuki Fukutani and Walter Herzog. "Current understanding of residual force enhancement: Cross-bridge component and non-cross-bridge component". In: *International Journal of Molecular Sciences* 20.21 (2019). ISSN: 14220067. DOI: 10.3390/ijms20215479.

[20] Daiani de Campos et al. "Residual force enhancement in human skeletal muscles: A systematic review and meta-analysis". In: *Journal of Sport and Health Science* 11.1 (2022), pp. 94–103. ISSN: 22132961. DOI: 10.1016/j.jshs.2021.05.006. URL: https://doi.org/10.1016/j.jshs.2021.05.006.

[21] Geoffrey A. Power et al. "The long and short of residual force enhancement non-responders". In: *European Journal of Applied Physiology* 120.12 (2020), pp. 2565–2567. ISSN: 14396327. DOI: 10.1007/s00421-020-04511-5. URL: https://doi.org/10.1007/s00421-020-04511-5.

[22] Z H Zhou and S Liu. *Machine Learning*. Springer Nature Singapore, 2021. ISBN: 9789811519673. URL: https://books.google.nl/books?id=ctM-EAAAQBAJ.

[23] Aaron E. Maxwell, Timothy A. Warner and Fang Fang. "Implementation of machine-learning classification in remote sensing: An applied review". In: *International Journal of Remote Sensing* 39.9 (2018), pp. 2784–2817. ISSN: 13665901. DOI: 10.1080/01431161.2018.1433343. URL: https://doi.org/10.1080/01431161.2018.1433343.

[24] Mahesh Batta. "Machine Learning Algorithms - A Review". In: *International Journal of Science and Research (IJSR)* 18.8 (2018), pp. 381–386. DOI: 10.21275/ART20203995.

[25] George Dimitoglou, James A. Adams and Carol M. Jim. "Comparison of the C4.5 and a Naive Bayes Classifier for the Prediction of Lung Cancer Survivability". In: (2012), pp. 1–9. URL: http://arxiv.org/abs/1206.1121.

[26] Vangelis Metsis, Ion Androutsopoulos and Georgios Paliouras. "Spam filtering with Naive Bayes - Which Naive Bayes?" In: *3rd Conference on Email and Anti-Spam - Proceedings, CEAS 2006* June 2014 (2006).

[27] Anthony Kelly and Marc Anthony Johnson. "Investigating the statistical assumptions of naïve bayes classifiers". In: *2021 55th Annual Conference on Information Sciences and Systems, CISS 2021* (2021). DOI: 10.1109/CISS50987.2021.9400215.

[28] Benyamin Ghojogh and Mark Crowley. "Linear and Quadratic Discriminant Analysis: Tutorial". In: 4 (2019), pp. 1–16. URL: http://arxiv.org/abs/1906.02590.

[29] Autcha Araveeporn. "Comparing the Linear and Quadratic Discriminant Analysis of Diabetes Disease Classification Based on Data Multicollinearity". In: *International Journal of Mathematics and Mathematical Sciences* 2022 (2022). ISSN: 16870425. DOI: 10.1155/2022/7829795.

[30] Efthymia Nikita and Panos Nikitas. "Sex estimation: a comparison of techniques based on binary logistic, probit and cumulative probit regression, linear and quadratic discriminant analysis, neural networks, and naïve Bayes classification using ordinal variables". In: *International Journal of Legal Medicine* 134.3 (2020), pp. 1213–1225. ISSN: 14371596. DOI: 10.1007/s00414-019-02148-4.

[31] David Aaron. Maroof. "Statistical methods in neuropsychology [electronic resource] : common procedures made comprehensible / David Aaron Maroof." In: (2012). URL: http://encore.lib.gla.ac.uk/iii/encore/record/C__Rb2938710__Sneuropsychology__Ff:facetmediatype:e:e:e-Book::__P0,13__Orightresult_U__X6?lang=eng&suite=cobalt.

[32] Sandro Sperandei. "Understanding logistic regression analysis". In: *Biochemia Medica* 24.1 (2014), pp. 12–18. ISSN: 13300962. DOI: 10.11613/BM.2014.003.

[33] Kaitlin ; Kirasich, Trace ; Smith and Bivin Sadler. "Random Forest vs Logistic Regression: Binary Classification for Heterogeneous Datasets". In: *SMU Data Science Review* 1.3 (2018), p. 9. URL: https://scholar.smu.edu/datasciencereviewAvailableat:https://scholar.smu.edu/datasciencereview/vol1/iss3/9http://digitalrepository.smu.edu..

[34] Javier M. Moguerza and Alberto Muñoz. "Support Vector Machines with Applications". In: *Statistical Science* (2006). DOI: 10.1214/088342306000000493.

[35] Jair Cervantes et al. "A comprehensive survey on support vector machine classification: Applications, challenges and trends". In: *Neurocomputing* 408 (2020), pp. 189–215. ISSN: 18728286. DOI: 10.1016/j.neucom.2019.10.118.

[36] Daniel T. Larose and Chantal D. Larose. "7.1 Classification Task". In: *Discovering Knowledge in Data: An Introduction to Data Mining*. 2nd ed. Wiley Data and Cybersecurity, 2014. Chap. k-Nearest, pp. 149–164. DOI: 10.1002/9781118874059.ch7.

[37] Liangxiao Jiang et al. "Survey of improving K-nearest-neighbor for classification". In: *Proceedings - Fourth International Conference on Fuzzy Systems and Knowledge Discovery, FSKD 2007* 1 (2007), pp. 679–683. DOI: 10.1109/FSKD.2007.552.

[38] Li Yu Hu et al. "The distance function effect on k-nearest neighbor classification for medical datasets". In: *SpringerPlus* 5.1 (2016). ISSN: 21931801. DOI: 10.1186/s40064-016-2941-7.

[39] Natalia Kosterina et al. "Muscular force production after concentric contraction". In: *Journal of Biomechanics* 41.11 (2008), pp. 2422–2429. ISSN: 00219290. DOI: 10.1016/j.jbiomech.2008.05.019.

[40] Rhiannan A.M. Pinnell et al. "Residual force enhancement and force depression in human single muscle fibres". In: *Journal of Biomechanics* 91 (2019), pp. 164–169. ISSN: 18732380. DOI: 10.1016/j.jbiomech.2019.05.025. URL: https://doi.org/10.1016/j.jbiomech.2019.05.025.

[41] Florian K. Paternoster et al. "Residual force enhancement in humans: Is there a true non-responder?" In: *Physiological Reports* 9.15 (2021). DOI: 10.14814/phy2.14944. URL: https://www.ptonline.com/articles/how-to-get-better-mfi-results.

[42] Atsuki Fukutani, Jun Misaki and Tadao Isaka. "Influence of joint angle on residual force enhancement in human plantar flexors". In: *Frontiers in Physiology* 8.APR (2017). ISSN: 1664042X. DOI: 10.3389/fphys.2017.00234.

[43] Jordan Grant et al. "Torque depression following active shortening is associated with a modulation of cortical and spinal excitation: a history-dependent study". In: *Physiological Reports* 5.15 (2017), pp. 1–10. ISSN: 2051817X. DOI: 10.14814/phy2.13367.

[44] Caleb T. Sypkes et al. "Spinal excitability is increased in the torque-depressed isometric steady state following active muscle shortening". In: *Royal Society Open Science* 4.11 (2017). ISSN: 20545703. DOI: 10.1098/rsos.171101.

[45] Alexis A. Jones, Geoffrey A. Power and Walter Herzog. "History dependence of the electromyogram: Implications for isometric steady-state EMG parameters following a lengthening or shortening contraction". In: *Journal of Electromyography and Kinesiology* 27 (2016), pp. 30–38. ISSN: 18735711. DOI: 10.1016/j.jelekin.2016.01.008. URL: http://dx.doi.org/10.1016/j.jelekin.2016.01.008.

[46] Kathryn A. Ramsey, Anthony J. Bakker and Gavin J. Pinniger. "Fiber-type dependence of stretch-induced force enhancement in rat skeletal muscle". In: *Muscle and Nerve* 42.5 (2010), pp. 769–777. ISSN: 0148639X. DOI: 10.1002/mus.21744.

[47] Atsuki Fukutani and Walter Herzog. "Differences in stretch-shortening cycle and residual force enhancement between muscles". In: *Journal of Biomechanics* 112 (2020). ISSN: 18732380. DOI: 10.1016/j.jbiomech.2020.110040.

[48] Atsuki Fukutani and Walter Herzog. "Residual force enhancement is attenuated for quick stretch conditions". In: *Journal of Biomechanics* 136.March (2022), p. 111076. ISSN: 18732380. DOI: 10.1016/j.jbiomech.2022.111076. URL: https://doi.org/10.1016/j.jbiomech.2022.111076.

[49] V. Joumaa et al. "Effects of fiber type on force depression after active shortening in skeletal muscle". In: *Journal of Biomechanics* 48.10 (2015), pp. 1687–1692. ISSN: 18732380. DOI: 10.1016/j.jbiomech.2015.05.023. URL: http://dx.doi.org/10.1016/j.jbiomech.2015.05.023.

[50] Stuart G. Campbell, P. Chris Hatfield and Kenneth S. Campbell. "A mathematical model of muscle containing heterogeneous half-sarcomeres exhibits residual force enhancement". In: *PLoS Computational Biology* 7.9 (2011). ISSN: 15537358. DOI: 10.1371/journal.pcbi.1002156.

[51] James M Wakeling, Míriam Febrer-Nafría and Friedl De Groote. "A review of the efforts to develop muscle and musculoskeletal models for biomechanics in the last 50 years". In: *Journal of Biomechanics* 155 (2023), p. 111657. ISSN: 0021-9290. DOI: https://doi.org/10.1016/j.jbiomech.2023.111657. URL: https://www.sciencedirect.com/science/article/pii/S0021929023002269.

[52] Craig P McGowan, Richard R Neptune and Walter Herzog. "A phenomenological model and validation of shortening-induced force depression during muscle contractions". In: *Journal of Biomechanics* 43.3 (2010), pp. 449–454. ISSN: 0021-9290. DOI: https://doi.org/10.1016/j.jbiomech.2009.09.047. URL: https://www.sciencedirect.com/science/article/pii/S0021929009005673.

[53] Stephanie A Ross, Nilima Nigam and James M Wakeling. "A modelling approach for exploring muscle dynamics during cyclic contractions". In: *PLOS Computational Biology* 14.4 (2018), pp. 1–18. DOI: 10.1371/journal.pcbi.1006123. URL: https://doi.org/10.1371/journal.pcbi.1006123.

[54] C P McGowan, R R Neptune and W Herzog. "A phenomenological muscle model to assess history dependent effects in human movement." eng. In: *Journal of biomechanics* 46.1 (Jan. 2013), pp. 151–157. ISSN: 1873-2380 (Electronic). DOI: 10.1016/j.jbiomech.2012.10.034.

[55] Stephanie A. Ross et al. "Size, history-dependent, activation and three-dimensional effects on the work and power produced during cyclic muscle contractions". In: *Integrative and Comparative Biology* 58.2 (2018), pp. 232–250. ISSN: 15577023. DOI: 10.1093/icb/icy021.

[56] Christian Rode, Tobias Siebert and Reinhard Blickhan. "Titin-induced force enhancement and force depression: A 'sticky-spring' mechanism in muscle contractions?" In: *Journal of Theoretical Biology* 259.2 (2009), pp. 350–360. ISSN: 00225193. DOI: 10.1016/j.jtbi.2009.03.015.

[57] Thomas Heidlauf et al. "A multi-scale continuum model of skeletal muscle mechanics predicting force enhancement based on actin–titin interaction". In: *Biomechanics and Modeling in Mechanobiology* 15.6 (2016), pp. 1423–1437. ISSN: 16177940. DOI: 10.1007/s10237-016-0772-7.

[58] Gudrun Schappacher-Tilp et al. "A novel three-filament model of force generation in eccentric contraction of skeletal muscles". In: *PLoS ONE* 10.3 (2015), pp. 1–16. ISSN: 19326203. DOI: 10.1371/journal.pone.0117634.

[59] Shahadat Uddin et al. "Comparing different supervised machine learning algorithms for disease prediction". In: *BMC Medical Informatics and Decision Making* 19.1 (2019), pp. 1–16. ISSN: 14726947. DOI: 10.1186/s12911-019-1004-8.

[60] Saloni Aneja and Sangeeta Lal. "Effective asthma disease prediction using naive Bayes — Neural network fusion technique". In: *2014 International Conference on Parallel, Distributed and Grid Computing* (2014), pp. 137–140. URL: https://api.semanticscholar.org/CorpusID:2838102.

[61] Turgay Ayer et al. "Informatics in radiology: comparison of logistic regression and artificial neural network models in breast cancer risk estimation." eng. In: *Radiographics : a review publication of the Radiological Society of North America, Inc* 30.1 (Jan. 2010), pp. 13–22. ISSN: 1527-1323 (Electronic). DOI: 10.1148/rg.301095057.

[62] Min Chen et al. "Disease Prediction by Machine Learning Over Big Data From Healthcare Communities". In: *IEEE Access* 5 (2017), pp. 8869–8879. DOI: 10.1109/ACCESS.2017.2694446.

[63] Sarul Malik et al. "Non-invasive detection of fasting blood glucose level via electrochemical measurement of saliva." eng. In: *SpringerPlus* 5.1 (2016), p. 701. ISSN: 2193-1801 (Print). DOI: 10.1186/s40064-016-2339-6.

[64] Rafael Anicet Zanini, Esther Luna Colombini and Maria Claudia Ferrari De Castro. "Parkinson's disease EMG signal prediction using neural networks". In: *Conference Proceedings - IEEE International Conference on Systems, Man and Cybernetics* 2019-Octob (2019), pp. 2446–2453. ISSN: 1062922X. DOI: 10.1109/SMC.2019.8914553.

[65] Alejandro Pascual-Valdunciel et al. "Classification of Kinematic and Electromyographic Signals Associated with Pathological Tremor Using Machine and Deep Learning". In: *Entropy* 25.1 (2023). ISSN: 10994300. DOI: 10.3390/e25010114.

[66] Wolfgang Seiberl et al. "On the relevance of residual force enhancement for everyday human movement". In: *Journal of Biomechanics* 46.12 (2013), pp. 1996–2001. ISSN: 00219290. DOI: 10.1016/j.jbiomech.2013.06.014. URL: http://dx.doi.org/10.1016/j.jbiomech.2013.06.014.

[67] V. Joumaa and W. Herzog. "Energy cost of force production is reduced after active stretch in skinned muscle fibres". In: *Journal of Biomechanics* 46.6 (2013), pp. 1135–1139. ISSN: 00219290. DOI: 10.1016/j.jbiomech.2013.01.008. URL: http://dx.doi.org/10.1016/j.jbiomech.2013.01.008.

[68] Robert K. Josephson and Darrell R. Stokes. "Work-dependent deactivation of a crustacean muscle". In: *Journal of Experimental Biology* 202.18 (1999), pp. 2551–2565. ISSN: 00220949. DOI: 10.1242/jeb.202.18.2551.

[69] Brent J. Raiteri, Leon Lauret and Daniel Hahn. *Residual Force Depression during submaximal voluntary contractions is not simply related to the preceding positive muscle work.* Fukuoka, 2023.

[70] Sebastian F. Baumbach et al. "The influence of knee position on ankle dorsiflexion - A biometric study". In: *BMC Musculoskeletal Disorders* 15.1 (2014), pp. 1–7. ISSN: 14712474. DOI: 10.1186/1471-2474-15-246.

[71] Marianne Boyer et al. "Reducing Noise, Artifacts and Interference in Single-Channel EMG Signals: A Review". In: *Sensors* 23.6 (2023), pp. 1–29. ISSN: 14248220. DOI: 10.3390/s23062927.

[72] Luciano Fernandes Crozara et al. "Motor readiness and joint torque production in lower limbs of older women fallers and non-fallers". In: *Journal of Electromyography and Kinesiology* 23.5 (2013), pp. 1131–1138. ISSN: 10506411. DOI: 10.1016/j.jelekin.2013.04.016. URL: http://dx.doi.org/10.1016/j.jelekin.2013.04.016.

[73] Mary Hellen Morcelli et al. "Neuromuscular performance in the hip joint of elderly fallers and non-fallers". In: *Aging Clinical and Experimental Research* 28.3 (2016), pp. 443–450. ISSN: 17208319. DOI: 10.1007/s40520-015-0448-7.

[74] Daniel Hahn et al. "Evidence of residual force enhancement for multi-joint leg extension". In: *Journal of Biomechanics* 43.8 (2010), pp. 1503–1508. ISSN: 0021-9290. DOI: https://doi.org/10.1016/j.jbiomech.2010.01.041. URL: https://www.sciencedirect.com/science/article/pii/S0021929010000825.

[75] Geoffrey A. Power, Charles L. Rice and Anthony A. Vandervoort. "Increased Residual Force Enhancement in Older Adults Is Associated with a Maintenance of Eccentric Strength". In: *PLoS ONE* 7.10 (2012). ISSN: 19326203. DOI: 10.1371/journal.pone.0048044.

[76] Chandramouli Krishnan and Glenn N. Williams. "Evoked Tetanic Torque and Activation Level Explain Strength Differences by Side". In: *Eur J Appl Physiol* 106.5 (2009), 769–774. ISSN: 0000000000. DOI: 10.1007/s00421-009-1057-y.

[77] Atsushi Takagi, Hiroyuki Kambara and Yasuharu Koike. "Independent control of cocontraction and reciprocal activity during goal-directed reaching in muscle space". In: *Scientific Reports* 10.1 (2020), pp. 1–9. ISSN: 20452322. DOI: 10.1038/s41598-020-79526-1. URL: https://doi.org/10.1038/s41598-020-79526-1.

[78] Todd Pataky. *SPM 1D.* 2022. URL: https://spm1d.org/.

[79] Jackey Chen and Geoffrey A. Power. "Modifiability of the history dependence of force through chronic eccentric and concentric biased resistance training". In: *Journal of Applied Physiology* 126.3 (2018), pp. 647–657. ISSN: 15221601. DOI: 10.1152/japplphysiol.00928.2018.

[80] Caleb T. Sypkes et al. "The influence of residual force enhancement on spinal and supraspinal excitability". In: *PeerJ* 2018.8 (2018), pp. 1–15. ISSN: 21678359. DOI: 10.7717/peerj.5421.

[81] Markus Tilp, S. Steib and W. Herzog. "Force-time history effects in voluntary contractions of human tibialis anterior". In: *European Journal of Applied Physiology* 106.2 (2009), pp. 159–166. ISSN: 14396319. DOI: 10.1007/s00421-009-1006-9.

[82] Avery Hinks et al. "Influence of isometric training at short and long muscle-tendon unit lengths on the history dependence of force". In: *Scandinavian Journal of Medicine and Science in Sports* 31.2 (2021), pp. 325–338. ISSN: 16000838. DOI: 10.1111/sms.13842.

[83] James Paquin and Geoffrey A. Power. "History dependence of the EMG-torque relationship". In: *Journal of Electromyography and Kinesiology* 41.May (2018), pp. 109–115. ISSN: 18735711. DOI: 10.1016/j.jelekin.2018.05.005.

[84] Atsuki Fukutani, Jun Misaki and Tadao Isaka. "Force depression in plantar flexors exists equally in plantar flexed and dorsiflexed regions". In: *Frontiers in Physiology* 8.MAR (2017), pp. 1–7. ISSN: 1664042X. DOI: 10.3389/fphys.2017.00183.

[85] Geoffrey A. Power et al. "Shortening-induced torque depression in old men: Implications for age-related power loss". In: *Experimental Gerontology* 57 (2014), pp. 75–80. ISSN: 18736815. DOI: 10.1016/j.exger.2014.05.004. URL: http://dx.doi.org/10.1016/j.exger.2014.05.004.

[86] Nicole Mazara et al. "Activation reduction following an eccentric contraction impairs torque steadiness in the isometric steady-state". In: *Journal of Sport and Health Science* 7.3 (2018), pp. 310–317. ISSN: 22132961. DOI: 10.1016/j.jshs.2018.05.001. URL: https://doi.org/10.1016/j.jshs.2018.05.001.

[87] Brian H. Dalton, Vincenzo S. Contento and Geoffrey A. Power. "Residual force enhancement during submaximal and maximal effort contractions of the plantar flexors across knee angle". In: *Journal of Biomechanics* 78 (2018), pp. 70–76. ISSN: 18732380. DOI: 10.1016/j.jbiomech.2018.07.019. URL: https://doi.org/10.1016/j.jbiomech.2018.07.019.

[88] Gavin J. Pinniger and Andrew G. Cresswell. "Residual force enhancement after lengthening is present during submaximal plantar flexion and dorsiflexion actions in humans". In: *Journal of Applied Physiology* 102.1 (2007), pp. 18–25. ISSN: 87507587. DOI: 10.1152/japplphysiol.00565.2006.

[89] Manuela Besomi et al. "Consensus for experimental design in electromyography (CEDE) project: Amplitude normalization matrix". In: *Journal of Electromyography and Kinesiology* 53.April (2020), p. 102438. ISSN: 18735711. DOI: 10.1016/j.jelekin.2020.102438. URL: https://doi.org/10.1016/j.jelekin.2020.102438.

[90] Duncan Reid et al. "Electromyographic analysis of an eccentric calf muscle exercise in persons with and without Achilles tendinopathy". In: *Physical Therapy in Sport* 13.3 (2012), pp. 150–155. ISSN: 1466853X. DOI: 10.1016/j.ptsp.2011.08.003.

[91] W. Herzog, L. J. Read and H. E.D.J. ter Keurs. "Experimental determination of force-length relations of intact human gastrocnemius muscles". In: *Clinical Biomechanics* 6.4 (1991), pp. 230–238. ISSN: 02680033. DOI: 10.1016/0268-0033(91)90051-Q.

[92] Jonas Rubenson et al. "On the ascent: The soleus operating length is conserved to the ascending limb of the force-length curve across gait mechanics in humans". In: *Journal of Experimental Biology* 215.20 (2012), pp. 3539–3551. ISSN: 00220949. DOI: 10.1242/jeb.070466.

[93] Alessio Gallina et al. "Consensus for experimental design in electromyography (CEDE) project: High-density surface electromyography matrix". In: *Journal of Electromyography and Kinesiology* 64 (2022), p. 102656. ISSN: 1050-6411. DOI: https://doi.org/10.1016/j.jelekin.2022.102656. URL: https://www.sciencedirect.com/science/article/pii/S1050641122000293.

[94] Andrea Casolo et al. "Non-invasive estimation of muscle fibre size from high-density electromyography". In: *Journal of Physiology* 601.10 (2023), pp. 1831–1850. ISSN: 14697793. DOI: 10.1113/JP284170.

[95] Alhanoof Althnian et al. "Impact of dataset size on classification performance: An empirical evaluation in the medical domain". In: *Applied Sciences (Switzerland)* 11.2 (2021), pp. 1–18. ISSN: 20763417. DOI: 10.3390/app11020796.

[96] Jie Cai et al. "Feature selection in machine learning: A new perspective". In: *Neurocomputing* 300 (2018), pp. 70–79. ISSN: 18728286. DOI: 10.1016/j.neucom.2017.11.077. URL: https://doi.org/10.1016/j.neucom.2017.11.077.

[97] In Lee and Yong Jae Shin. "Machine learning for enterprises: Applications, algorithm selection, and challenges". In: *Business Horizons* 63.2 (2020), pp. 157–170. ISSN: 00076813. DOI: 10.1016/j.bushor.2019.10.005. URL: https://doi.org/10.1016/j.bushor.2019.10.005.

Appendix

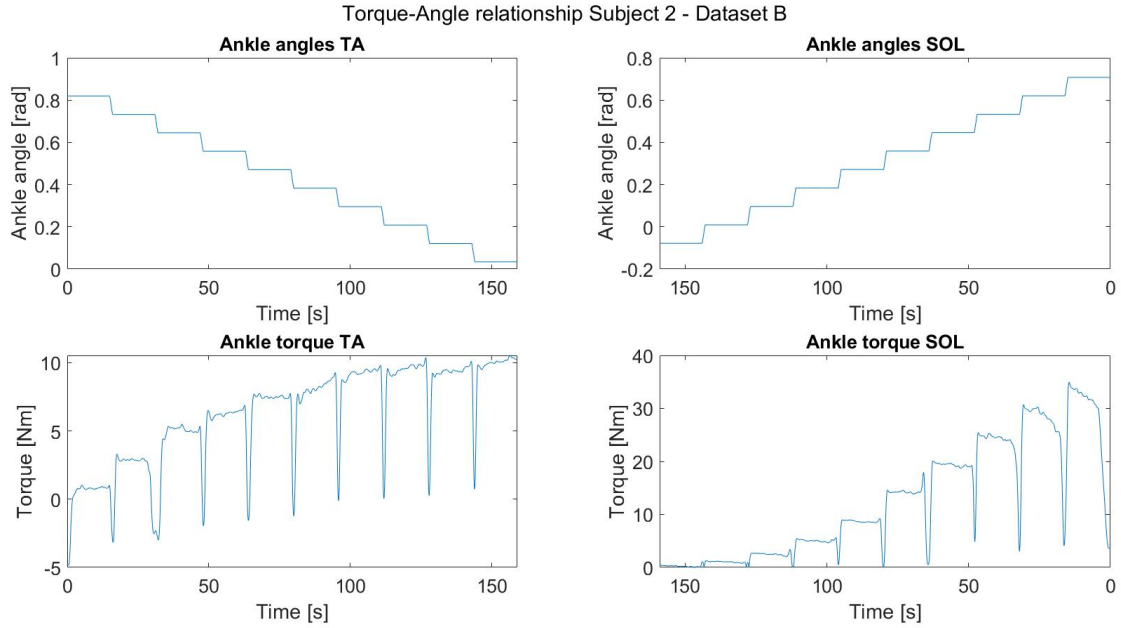## A. Torque-angle relationship

Figure 20: Torque-angle relationship of both the TA and the SOL of subject 2 of dataset B with increasing muscle length. The trial measured the torque at ten different angle angles while the subject was sub-maximally contracting at 7.5-12.5 %MVC. For dataset B it was attempted to measure rFE and rFD at the plateau region. The selected ankle angles were for the TA at 0.0311 rad and for the SOL at 0.3340 rad where 0 rad is the natural configuration of the footplate of the Achilles Perturbator (horizontal).

B. Selected trials

Table 4: Overview of the selected combinations of trials for both datasets.

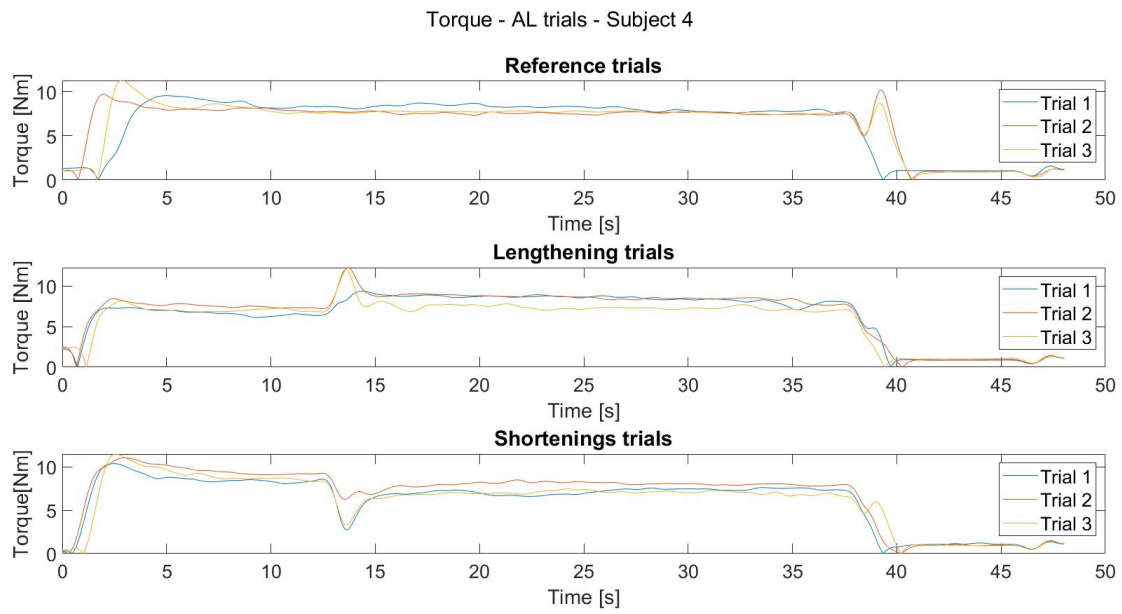| | Dataset A | | | | | | | Dataset B | | | | | |
	Ascending limb			Plateau region				Tibialis Anterior			Soleus		
	Ref	Length	Short	Ref	Length	Short		Ref	Length	Short	Ref	Length	Short
SBJ1	3	3	2	1	1	3	SBJ2	1	2	1	3	1	3
SBJ2	3	3	2	2	1	3	SBJ3	3	2	1	1	1	2
SBJ3	1	2	1	3	1	3	SBJ4	3	2	2	3	2	3
SBJ4	2	2	1	3	1	3	SBJ5	2	1	2	2	2	2
SBJ5	3	3	2	2	1	1	SBJ6	1	2	2	3	1	3

C. Torque profile

Figure 21: The torque profile of subject 4 of dataset A measured at the ascending limb over the entire times series.